Redox Biology 75 (2024) 103262

Contents lists available at ScienceDirect

Redox Biology

journal homepage: www.elsevier.com/locate/redox

ABCG2 shields against epilepsy, relieves oxidative stress and apoptosis via inhibiting the ISGylation of STAT1 and mTOR

Chang Li [a,b,c,1], Yi Cai [a,c,1], Yongmin Chen [d], Jingyi Tong [a,c], Youbin Li [b], Dong Liu [b], Yun Wang [a,c], Zhiping Li [e,f,**], Yan Wang [a,b,*], Qifu Li [a,c,***]

[a] Department of Neurology, The First Affiliated Hospital of Hainan Medical University, Hainan Key Laboratory for Research and Development of Tropical Herbs, Engineering Research Center of Tropical Medicine Innovation and Transformation of Ministry of Education, School of Pharmacy, Hainan Medical University, Haikou, China

[b] International Joint Research Center of Human-machine Intelligent Collaborative for Tumor Precision Diagnosis and Treatment of Hainan Province, Haikou Key Laboratory of Li Nationality Medicine, School of Pharmacy, Hainan Medical University, Haikou, China

[c] Key Laboratory of Brain Science Research & Transformation in Tropical Environment of Hainan Province, Hainan Medical University, Haikou, China

[d] Department of Functional Diagnosis, The Second Affiliated Hospital of Hainan Medical University, Haikou, China

[e] Department of Clinical Pharmacy, Children's Hospital of Fudan University, National Children's Medical Center, Shanghai, China

[f] Department of Clinical Pharmacy, Kunshan Maternity and Children's Health Care Hospital, Children's Hospital of Fudan University Kunshan Branch, Kunshan, Jiangsu, China

ARTICLE INFO

Keywords:
Epilepsy
ABCG2
Oxidative stress
Apoptosis
ISGylation

ABSTRACT

The transporter protein ABC subfamily G member 2 (ABCG2) is implicated in epilepsy; however, its specific role remains unclear. In this study, we assessed changes in ABCG2 expression and its role in epilepsy both *in vitro* and *in vivo*. We observed an instantaneous increase in ABCG2 expression in epileptic animals and cells. Further, ABCG2 overexpression significantly suppressed the oxidative stress and apoptosis induced by glutamate, kainic acid (KA), and lipopolysaccharide (LPS) in neuronal and microglia cells. Furthermore, inhibiting ABCG2 activity offset this protective effect. ABCG2-deficient mice ($ABCG2^{-/-}$) showed shorter survival times and decreased survival rates when administered with pentylenetetrazole (PTZ). We also noticed the accumulation of signal transducer and activator of transcription 1 (STAT1) and decreased phosphorylation of mammalian target of rapamycin kinase (mTOR) along with increased ISGylation in $ABCG2^{-/-}$ mice. ABCG2 overexpression directly interacted with STAT1 and mTOR, leading to a decrease in their ISGylation. Our findings indicate the rapid increase in ABCG2 expression acts as a shield in epileptogenesis, indicating ABCG2 may serve as a potential therapeutic target for epilepsy treatment.

1. Introduction

Epilepsy is a common neurological disorder characterized by abnormal brain discharge that leads to recurrent limb twitching and loss of consciousness, affecting approximately 1 % of the global population. Currently, antiseizure medication (ASM) therapy is the main treatment for epilepsy. However, approximately 30 % of patients remain medically intractable, which imposes a heavy economic burden on both patients and society [1].

ATP-binding cassette (ABC) transporters are a superfamily of proteins that utilize the chemical energy derived from ATP hydrolysis to translocate various compounds across biological membranes, including uric acid and many commonly prescribed anticancer drugs [2,3]. Two of extensively studied ABC transporters, subfamily B member 1 (ABCB1; P-glycoprotein) and ABC subfamily G member 2 (ABCG2; BCRP), regulate the absorption of substrate drugs in the intestinal epithelium and their distribution across the blood-brain barrier (BBB) and the blood-placental barrier (BPB). Absolute quantity proteomic analysis has

* Corresponding author. Hainan Key Laboratory for Research and Development of Tropical Herbs, School of Pharmacy, Hainan Medical University, No. 3 Xueyuan Road, Haikou, 571199, China.

** Corresponding author. Department of Clinical Pharmacy, Children's Hospital of Fudan University, 399 Wanyuan Road, Shanghai, 201102, China.

*** Corresponding author. Department of Neurology, The First Affiliated Hospital of Hainan Medical University, 31 Longhua Road, Haikou, 570102, China.

E-mail addresses: zpli@fudan.edu.cn (Z. Li), hy0207116@hainmc.edu.cn (Y. Wang), lee-chief@163.com (Q. Li).

[1] These authors contributed equally to this work.

https://doi.org/10.1016/j.redox.2024.103262
Received 31 May 2024; Received in revised form 27 June 2024; Accepted 28 June 2024
Available online 4 July 2024

demonstrated that the protein expression of ABCG2 is higher than that of ABCB1 in the brain microvessels of epileptic patients [4].

Since ABCG2 was first discovered in 1998, an increasing number of studies have focused on its pharmacogenomics and expression in epilepsy [5]. *ABCG2* polymorphisms at rs2231137 are closely related to drug-resistant epilepsy [6]. Further, protein expression of ABCG2 was significantly increased in the brains of rats administered 50 mg/kg pentylenetetrazole (PTZ) [7] and in the hippocampi of rats that underwent tetanic stimulation in the latent period and chronic epileptic phase [8]. Moreover, lamotrigine (LTG), a commonly used antiepileptic drug, is a substrate of ABCG2. This observation suggests that ABCG2 causes extra transport of LTG, leading to resistance to LTG [9]. Contrary to expectations, polymorphisms of *ABCG2*, including 421C > A, rs2231137, rs2231142, and rs3219191, were not found to be associated with drug-resistance epilepsy [10,11]. Interestingly, ABCG2 expression levels do not change in the tissues of patients with hippocampal sclerosis or focal cortical dysplasia [8,12]. Specially, Weidner et al. demonstrated higher protein expression of ABCG2 in the hippocampi of patients with non-drug-resistant mesial temporal lobe epilepsy (non-MTLE) compared to those with MTLE patients [13]. Considering the above information, it is crucial to determine the expression and role of ABCG2 in epilepsy. Here we show that PTZ and kainic acid (KA) instantaneously increased expression of ABCG2 in rats and mice, along with seizure activity. This phenotype is primarily obeserved in neurons as well as in microglia, which acts as a shield to prevent neurons and microglia from oxidative stress and apoptosis. In addition, we identified that ABCG2 directly bined with the signal transducer and activator of transcription 1 (STAT1) and the mammalian target of rapamycin kinase (mTOR), decreased ISGylation of mTOR and STAT1. Further, deficiency of ABCG2 caused accumulation of STAT1 and decreased phosphorylation of mTOR with increasing ISGylation. Overall, this study indicates that ABCG2 shields against epilepsy and thus may serve as a potential target for treating epilepsy.

2. Materials and methods

2.1. Animals

Male Sprague−Dawley rats and C57BL/6J mice (certificate no. SCXK2014-0011) at 8 weeks of ages were obtained from Tianqin Biotechnology Co., Ltd. (Hunan, China). The animals were housed in plastic cages under illumination (12-h light/12-h dark) conditions and fed a standard pelleted chow diet. We followed the instructions of the Animal Research Reporting of In Vivo Experiment (ARRIVE) Guidelines 2.0 [14] and efforts were made to reduce the number of animals used and minimize animal suffering. This study was approved by the Ethics Committee of Animal Care at our institute (No. HYLL-2021-190).

ABCG2$^{-/-}$ mice with a C57BL/6J background were constructed by Shanghai Model Organisms Center Inc. Using a CRISPR/Cas9 system with gRNA-T2 and hCas9. The analysis was performed on 4- to 9-week-old females and males.

2.2. PTZ-induced and KA-induced epilepsy

Rats were administered a subconvulsive dose (35 mg/kg) of PTZ (Roche, Switzerland) by intraperitoneal (i.p.) injection for 28 days to treat chronic epilepsy or with 60 mg/kg of PTZ to induce acute seizures. Mice were administered by a subconvulsive dose (15 mg/kg, i.p.) of KA (Sigma, USA) to induce epilepsy, and seizures were observed on the 3rd, 5th, 7th, 14th, and 30th days. Seizures were scored according to Racine's criteria [15], while, latency to seizure onset was defined as the time elapsed between the PTZ or KA injection and the first observed seizure response [16]. Fully kindled rats with stage three seizures after three consecutive PTZ injections were selected for the subsequent experiments [17,18].

2.3. Open-field test

The open-field test was used to evaluate locomotor activity. Mice were placed at the periphery of the arena and allowed to explore the arena for 5 min. The time spent in the center of the open field was recorded and analyzed using VisuTrack software (Shanghai Xin Ruan MDT infotech LTD, Shanghai, China). It is currently acknowledged that that the number of crossing the central area indicates exploratory behavior and anxiety [19].

2.4. Cell culture and transfection

The murine hippocampal (HT22, #337709) and microglial (BV2, #CL-0493A) cell lines were purchased from the Bena Culture Collection (Henan, China) and Pricella (Wuhan, Hubei, China), respectively. Cells were cultured in high glucose Dulbecco's modified Eagle's medium (DMEM; Gibco, Carlsbad, CA, USA) supplemented with 10 % fetal bovine serum (CLARK, Richmond, VA, USA) and 1 % streptomycin/penicillin (Biosharp, Anhui, China) in a humidified incubator with 5 % CO_2 at 37 °C.

The hABCG2 overexpression plasmid was designed and manufactured by Shanghai GeneChem Co., Ltd. (Shanghai, China) and further transfected into HT22 and BV2 cells using Lipofectamine 3000 (Invitrogen, California, CA, USA).

2.5. Cell viability assay

Cells were plated at a density of 1×10^5 cells/well for 24 h, followed by treatment with various concentrations of glutamate (1, 5, 10, and 20 mM; Sigma) or LPS (1, 2, 5, and 10 μg/mL; Beyotime, Shanghai, China) or KA (150, 300, and 600 μM; MedChemExpress, New Jersey, NJ, USA) for 12 or 24 h. Then, each well was incubated with 20 μL of Cell Counting Kit-8 reagent (Dojindo, Kumamoto, Japan) at 37 °C for 30 min. Absorbance was measured using a microplate reader (Spectra MAX 190, Molecular Devices, San Jose, CA, USA) at 450 nm, as previously described [20].

2.6. Hoechst 33,258 staining

The chromatin-specific dye Hoechst 33,258 was used to visualize the morphological alterations in neurons and microglia. Briefly, cells were fixed with 4 % paraformaldehyde for 30 min, washed three times with phosphate-buffered saline (PBS), and incubated with Hoechst working solution (#C0003, Beyotime) for 15 min. The cells were observed and photographed under a magnification microscope (Zeiss X-Cite, Germany).

2.7. Lactate dehydrogenase (LDH) assay

The LDH content was detected using a diagnostic kit (Jiancheng Bioengineering Institute, Jiangsu, China) and calculated by using a microplate reader (Spectra MAX 190) at 450 nm.

2.8. Measurement of reactive oxygen species (ROS) generation, apoptosis, and iron content

2′,7′-dichlorofluorescin diacetate (H2DCFDA, Sigma), annexin V (Beyotime), and FerroOrange (GLPBIO, Montclair, CA, USA) were applied to detect ROS, apoptosis, and ferric ion content, respectively, according to the manufacturer's instructions. The cells were harvested using trypsin and incubated with the working solution at 37 °C for 30 min. The fluorescent intensity was detected by flow cytometry (NovoCyte, Agilent, Santa Clara, CA, USA) at phycoerythrin (PE) channel for annexin V, at allophycocyanin (APC) channel for H2DCFDA and FerroOrange.

2.9. Quantitative real-time PCR (qPCR)

Total RNA was extracted from the brains and cells and converted to cDNA using Reverse Transcriptase (Monad, Shanghai, China), followed by SYBR Green PCR (Monad) with specific primers (Table 1) according to the manufacturer's protocol. All samples were amplified in triplicate and the mRNA level was calculated using the $2^{-\Delta\Delta Ct}$ method with the expression level of *GAPDH* or *actin* as the references for rats and mice, respectively.

2.10. Western blot (WB)

Brain tissue or cells were lysed with a protein lysis buffer containing a phosphatase inhibitor (Boster, Hubei, China). Proteins were transferred onto polyvinylidene difluoride membranes, followed by blocking with QuickBlock (#P0256, Beyotime). Membranes were incubated with primary antibodies (Table 2) at 4 °C overnight, and hatched with secondary antibodies at 37 °C for 1 h. The results were visualized and quantified using a chemiluminescence detection system (Bio-Rad Laboratories, Inc., Hercules, CA, USA) and ImageJ software (version 1.52a; Wayne Rasband, Bethesda, USA), respectively.

2.11. Co-immunoprecipitation (COIP)

Cell lysates from HT22 or tissues were obtained using ice-cold lysis buffer followed by centrifuged at 14,000×*g* for 10 min at 4 °C. Subsequently, the magnetic beads (Beyotime) were conjugated with the anti-STAT1, mTOR, and ABCG2 at 4 °C for 2 h, followed by incubation with lysates overnight at 4 °C with rotation. Then, the immunoprecipitated proteins were eluted and subjected to SDS-PAGE and immunoblotting using the indicated antibodies.

2.12. Immunofluorescence microscopy

Brain slices and cells were blocked with 5 % bovine serum albumin in PBS for 30 min, followed by incubated with primary antibody overnight at 4 °C. Then, brain slices and cells were stained with 4', 6-diamidino-2-phenylindole (DAPI, Boster) at 37 °C for 5 min. A magnification microscope (Zeiss X-Cite) was used to observe the stained cells, and images were processed using the ImageJ software (1.52a, Wayne Rasband, USA) [21].

2.13. Proteomics analysis

The hippocampi of ABCG2$^{-/-}$ mice and wildtype (WT) mice were ground with liquid nitrogen and dissolved by lysis buffer (8 M urea, 1 % protease inhibitor cocktail), followed by sonication on ice. The supernatant was collected after centrifugation at 12,000×*g* at 4 °C for 10 min, and the protein concentration was checked using BCA kit (Beyotime) according to the manufacturer's instructions. Protein samples were added to 20 % (m/v) trichloroacetic acid and incubated for 2 h at 4 °C, followed by washing with pre-cooled acetone and dried for 1 min. Protein was dissolved with 200 mM triethylammonium bicarbonate and digested by trypsin at 1:50 trypsin-to-protein mass ratio, followed by reduction with 5 mM dithiothreitol for 30 min at 56 °C, after that, 11 mM of iodoacetamide was added for 15 min at 25 °C in darkness to alkylate. The tryptic peptides were dissolved in solvent A (0.1 % formic acid, 2 % acetonitrile/in water) and loaded onto a home-made reversed-phase analytical column (25 cm length, 100 μm i.d.). Peptides were separated using a continuous gradient with solvents A and B (0.1 % formic acid in acetonitrile) at a constant flow rate of 450 nL/min on a NanoElute UHPLC system (Bruker Daltonics, Gemany). They were then subjected to a capillary source followed by time-of-flight (TOF) mass spectrometry (Bruker). The mass spectrometry parameters were as follows: The electrospray voltage was set to 1.6 kV, and data-independent parallel accumulation serial fragmentation (DIA-PASEF) mode was applied with 100–1700 *m/z* of the full MS scan. Meanwhile, 10PASEF-MS/MS scans were performed per cycle. The MS/MS scan range was set to 400–1200 *m/z* and the isolation window was set to 25 *m/z*.

DIA data were processed using the DIA-NN search engine (v1.8). Tandem mass spectra were searched against Musmusculus_10,090_sp_20230103, fasta (17,132 entries) and concatenated with the reverse-decoy database. Trypsin/P was specified as the cleavage enzyme, allowing for up to one missing cleavage. Excision of the *N*-terminal Met and carbamidomethyl on Cys was specified as a fixed modification, and the FDR was adjusted to <1 %. Proteins that reached the threshold (fold change >1.2 or < 0.83) were defined as differentially expressed proteins (DEPs).

Kyoto Encyclopedia of Genes and Genomes (KEGG) and Gene Ontology (GO) enrichment analyses were performed using Gene Set Enrichment Analysis (GSEA) with a pre-ranked list of fold-change values between ABCG2$^{-/-}$ and WT mice. Normalized enrichment scores (NES) with the total protein list were determined as the background, and parameters (n = 1000 permutations, max size = 500, min size = 10) were used. Statistical significance was set at $P < 0.05$. The protein-protein interaction (PPI) network of DEPs with high confidence (>0.7) was obtained using the STRING online tool (https://string.db.org) and visualized using Cytoscape v3.9.1 (https://www.cytoscape.org).

2.14. Statistical analysis

Data are expressed as mean ± standard error mean (SEM). Normality of the data was first tested using the Shapiro–Wilk test. Normally distributed data were analyzed using one-way analysis of variance (ANOVA) for multiple groups and the Student's t-test for two groups. Non-normally distributed data were analyzed using the Kruskal–Wallis test. Statistical analysis and figure generation were performed using

Table 2
Information of antibodies.

Antibody	Source	Identifier	Dilution Rate
Rabbit *anti*-ABCG2	Abcam	ab207732	1: 1000
Rabbit anti-STAT1	Proteintech	10144-2-AP	1: 1000
Mouse *anti*-p-STAT1	SANTA	sc-136229	1: 100
Mouse *anti*-p-mTOR	Proteintech	67778–1-Ig	1: 5000
Rabbit *anti*–HIF–1 *α*	Abcam	ab179483	1: 5000
Rabbit *anti*-mTOR	Abcam	ab2732	1: 2000
Rabbit *anti*-ISG15	Proteintech	15981-1-AP	1: 1000
Rabbit *anti*-CHOP	Proteintech	15204-1-AP	1: 1000
Rabbit *anti*-GAPDH	Proteintech	10494–1-AP	1: 6000

Table 1
Sequence and length of primers.

Gene names	Primer-F (5′-3′)	Primer-R (5′-3′)	Length (bp)
Actin	CCACAGCTGAGAGGGAAATC	AAGGAAGGCTGGAAAAGAGC	193
GAPDH	GGCATCCTGGGCTACACT	CCACCACCCTGTTGCTGT	163
ABCG2 for KO mice	TCGCAGAAGGAGATGTG	GCATTAAGGCCAGGTTTCATG	136
mABCG2	CTGAGGAATCACACCATCCAAC	TCCGGACTAGAAACCCACTCT	299
rABCG2	CCACTGGAATGCAAAATAGAG	CCTCATAGGTAGTAAGTCAGACACA	188
mSTAT1	GCCGAGAACATACCAGAGAATC	GATGTATCCAGTTCGCTTAGGG	141
mISG15	TGCCTGCAGTTCTGTACCAC	AGTGCTCCAGGACGGTCTTA	84

GraphPad Prism (Version 9.0.0, San Diego, CA, USA) and R language (Version 3.5.3, R Foundation for Statistical Computing, Vienna, Austria), respectively. Results were considered significant at $P < 0.05$.

3. Results

3.1. Seizure-induced instant overexpression of ABCG2 in vivo

A high dose of PTZ (60 mg/kg), a GABA(A) antagonist, was administered to induce acute seizures. In addition, a subconvulsive dose of PTZ (35 mg/kg) was used to induce chronic seizures [22] (Fig. 1A). The results showed that the mRNA expression of *ABCG2* was significantly increased in the hippocampi of acute-seizure rats but not in chronic-seizure rats, compared to the control group treated with saline (Fig. 1B). However, the protein expression of ABCG2 remarkably increased in the hippocampi of acute-seizure and chronic-seizure rats (Fig. 1C and D). Further, no change in the cortical tissues of rats was observed (Fig. 1E and F). Similar results were confirmed in PTZ-induced acute epileptic mice, in which the protein expression of ABCG2 was approximately two-fold higher than that in control mice (Fig. 1G and H), suggesting that the phenomenon of ABCG2 overexpression was not limited to species. We determined the instant expression of ABCG2 by using KA, an analog of glutamate, to induce chronic seizure in mice [23] (Fig. 1I). Mice chronically administered KA showed fewer central circle periods in the open field test on days 7 and 30 (Fig. 1J), in accordance with the increases in *ABCG2* mRNA expression over the first seven days (Fig. 1K) and protein expression on the 7th day (Fig. 1L). Collectively, these results suggested that interference with the glutamate and GABA axis induced protein expression of ABCG2.

We performed double immunohistochemistry in the cortex, CA1, and CA3 regions of the hippocampi using neuronal nuclei (NeuN), glial fibrillary acidic protein (GFAP), and the ionized calcium-binding

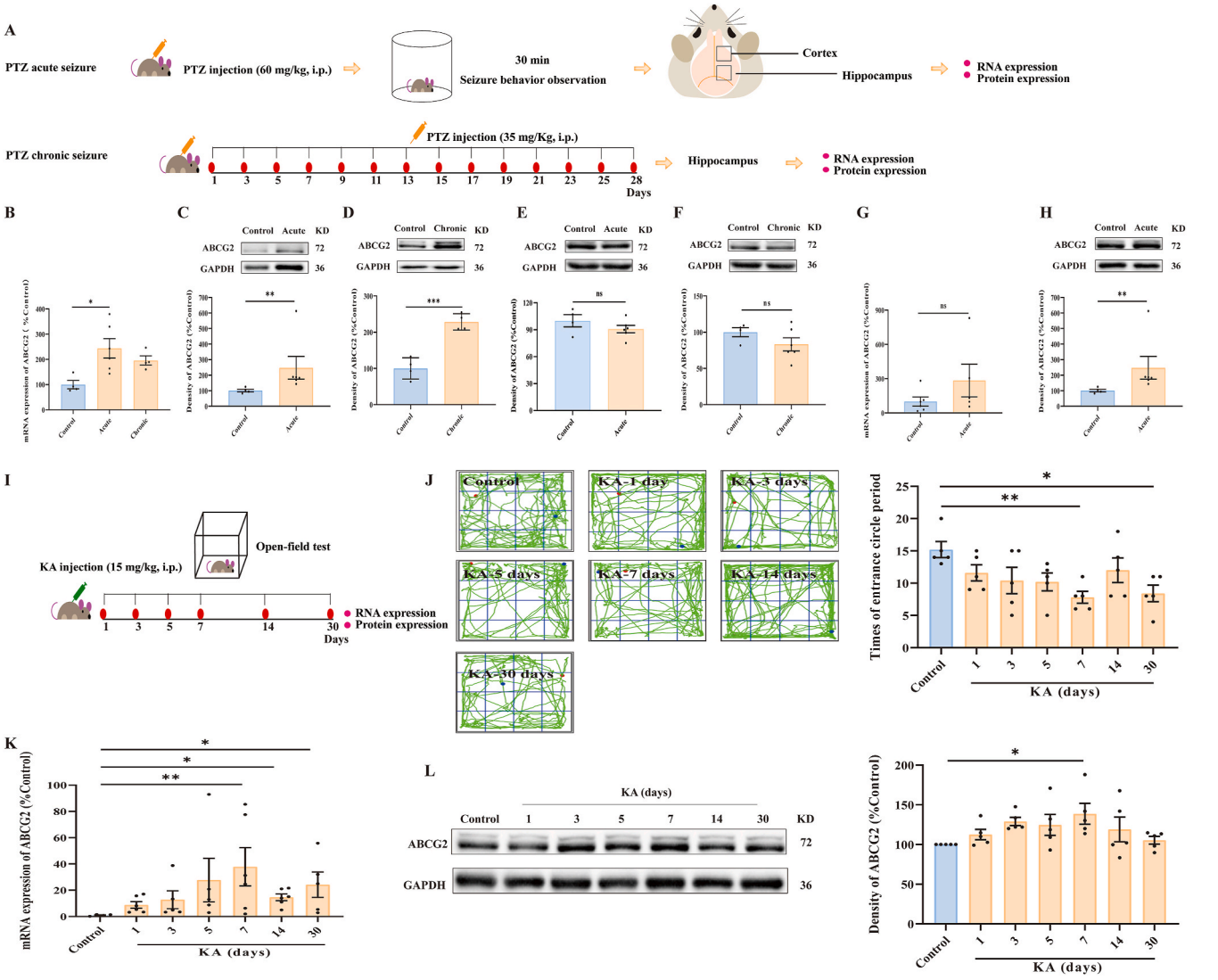

Fig. 1. Instantly increased expression of ABCG2 in the hippocampi of PTZ-induced acute, chronic rats, and KA-induced epileptic mice. **(A)** Procedure of acute and chronic epileptic rats administered by 60 mg/kg and 35 mg/kg of PTZ. **(B)** mRNA expression of *ABCG2* in the hippocampi of acute and chronic rats (Control group, $n = 4$; acute group, $n = 6$; chronic group, $n = 4$). **(C-D)** Protein expression of ABCG2 in the hippocampi of acute (**C**, $n = 6$) and chronic (**D**, $n = 4$) epileptic rats. **(E-F).** Protein expression of ABCG2 in the cortex of acute (**E**, Control group, $n = 4$; acute group, $n = 6$) and chronic (**F**, Control group, $n = 4$; chronic group, $n = 6$) epileptic rats. **(G-H)** mRNA expression (**G**) and protein expression (**H**) of ABCG2 in the hippocampi of PTZ-induced mice (Control group, $n = 6$; acute group, $n = 5$). **(I)** Procedure of KA-induced epileptic rats. **j** Open-field test at mice untreated by KA or administered by KA on the 1st day, 3rd day, 5th day, 7th day, 14th day, and 30th day ($n = 5$ per group). **(K-L)** The mRNA expression (**K**, $n = 5$ per group) and protein expression (**L**, $n = 5$ per group) of ABCG2 in the hippocampi of KA-induced epileptic mice. Data are presented as means ± SEM. Results designated with ns were not significant, whereas those designated with * ($P < 0.05$), ** ($P < 0.01$), ***($P < 0.001$) were significant according to adjusted P values in each indicated comparison.

adapter molecule (IBA1), which are specific to neurons, astrocytes, and microglia, respectively, to determine which cells expressed ABCG2. The results demonstrated that ABCG2 was mainly co-expressed in neurons and weakly expressed in microglia but not in astrocytes (Fig. S1).

3.2. Epilepsy-associated stimulators induced overexpression of ABCG2 in neurons and microglia in vitro

We explored the ABCG2 expression *in vitro* using glutamate and KA to mimic epilepsy. The results indicated that HT22 cell survival was not affected by glutamate administration (1–20 mM) for 24 h (Fig. S2A). Conversely, 300 or 600 μM of KA induced cell death, but not 150 μM (Fig. S2B). Cells pretreated with KA for 12 and 24 h induced the release of LDH and DNA fragments (Figs. S2C and D), which confirmed KA-induced injury. Therefore, 5 mM glutamate and 150 μM kA were used in subsequent experiments. Cells treated with 5 mM glutamate for 24 h showed significantly increased ABCG2 protein expression (Fig. 2A). Long-term stimulation with glutamate (96 h) and KA (24 h) significantly increased the mRNA expression of *ABCG2* (Fig. 2B and C). Further, the protein expression of ABCG2 was instantly induced by glutamate at 12 and 24 h, smoothly decreased at 48 and 72 h, and reached normal expression at 96 h (Fig. 2D). Additionally, neurons pretreated with KA for 12 and 24 h increased in ABCG2 protein expression to 1.5 times than that in the control group (Fig. 2E).

Microglia are another type of cell in the brain that induce immune reactions and are associated with epilepsy [24]. In this study, firstly, we also confirmed that 1–10 μg/mL of LPS and 150–600 μM of KA promoted the proliferation of BV2 (Figs. S2E and F). While 1 μg/mL of LPS and 150 μM of KA dramatically induced the ROS (Fig. S2G) and apoptosis of BV2 (Fig. S2H). With these stimulators, the mRNA expression of *ABCG2* was induced by BV2 cells in accordance with the overexpression of ABCG2 protein (Fig. 2F–I). This phenomenon indicated that

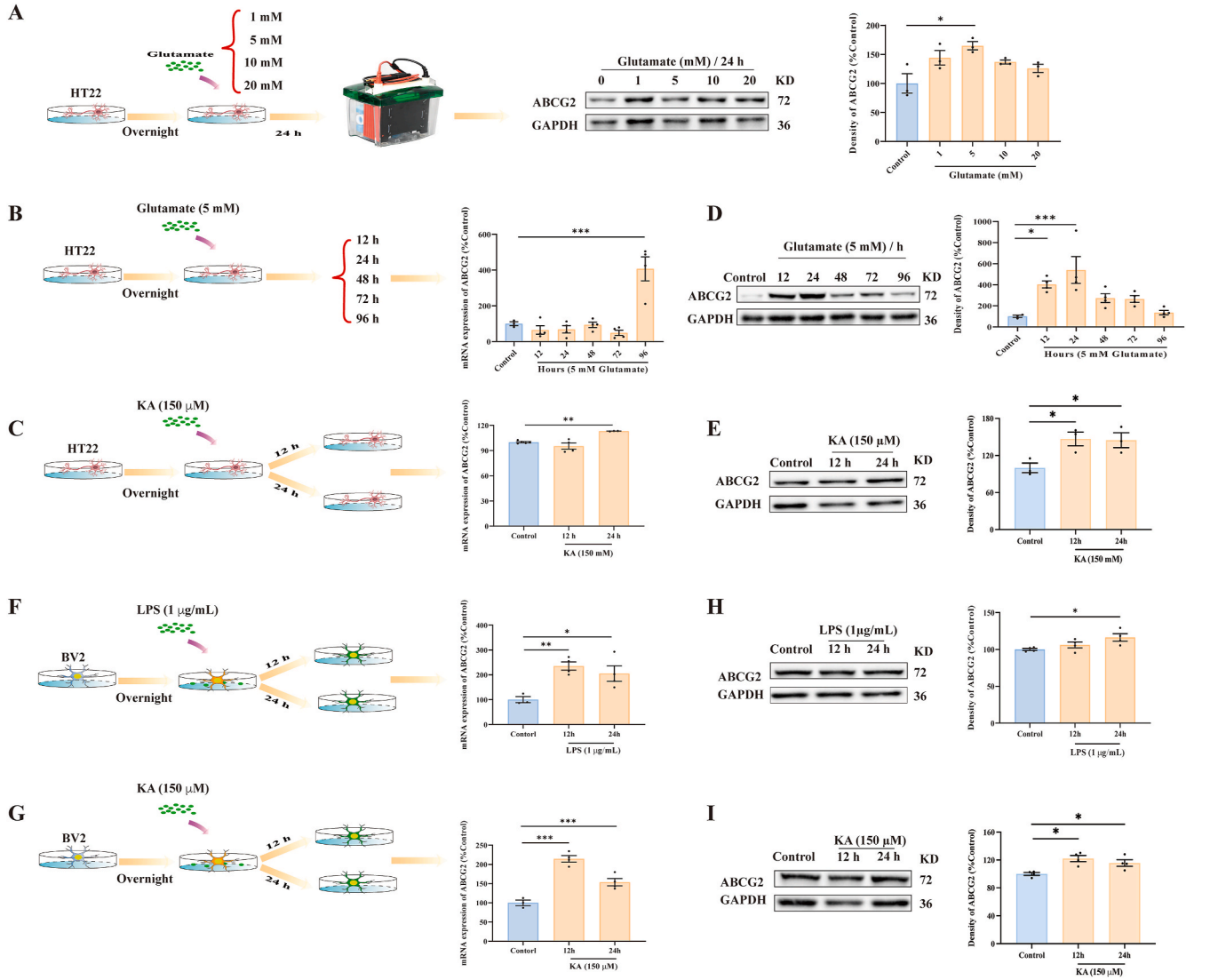

Fig. 2. Increased expression of ABCG2 in glutamate and KA-induced injury of mouse neuron (HT22) and LPS and KA-induced microglia (BV2). **(A)** Protein expression of ABCG2 in HT22 treated with 1, 5, 10, and 20 mM of glutamate for 24 h (0 μM group, $n = 3$; 1–20 μM groups, $n = 4$). **(B–C)** mRNA expression of *ABCG2* in HT22 treated with 5 mM of glutamate for 12, 24, 48, 72, and 96 h (**B**, Control group, $n = 3$; 12–96 h groups, $n = 4$) or treated with KA for 12 h and 24 h (**C**, Control group, $n = 5$; 12 h group, $n = 4$; 24 h group, $n = 3$). **(D-E)** Protein expression of ABCG2 in HT22 treated with 5 mM of glutamate for 12, 24, 48, 72, and 96 h (**D**, Control group, $n = 3$; 12–96 h groups, $n = 4$) or treated with KA for 12 and 24 h (**E**, $n = 3$ per group). **(F-G)** mRNA of *ABCG2* in BV2 treated with 1 μg/mL of LPS for 12 and 24 h (**F**, Control group, $n = 3$; 12 and 24 h groups, $n = 4$) or treated with KA for 12 and 24 h (**G**, Control group, $n = 3$; 12 and 24 h groups, $n = 4$). **(H–I)** Protein expression of ABCG2 in BV2 treated with 1 μg/mL of LPS for 12 and 24 h (**H**, $n = 4$ per group) or treated with KA for 12 and 24 h (**I**, $n = 4$ per group). Data are presented as means ± SEM. Results designated with * ($P < 0.05$), ** ($P < 0.01$), ***($P < 0.001$) were significant according to adjusted P values in each indicated comparison.

epilepsy-associated stimulators, including LPS and KA, immediately induced expression of ABCG2 *in vitro*.

3.3. Overexpression of ABCG2 in HT22 and BV2 prevents oxidative stress and apoptosis

We made an ABCG2-overexpressed plasmid and transferred it to HT22 cells to determine whether the overexpression of ABCG2 acts as a sword or shield in epilepsy (Fig. 3A). HT22 cells transfected with ABCG2-overexpressing plasmid or an empty plasmid whose concentrations varied from 2 to 8 μg for 24 h did not affect the survival rate of HT22 cells compared with the lipo3000 group (Fig. S3A). Transfected cells treated with glutamate (5 mM) for another 12 h did not affect the survival rate compared to the lipo3000 group (Fig. S3B). In the empty group (pUC-EP), cells administered glutamate showed a significantly increased release of LDH, ROS content, membrane distribution of annexin V, and ferric ion content, suggesting glutamate-induced neuronal excitotoxicity. However, cells transfected with 2 μg of ABCG2 offset the increase of LDH, ROS, apoptosis, and ferric ion (Fig. 3B–E).

We further confirmed the effect of ABCG2 on microglial BV2 cells. Briefly, BV2 cells transfected with plasmid for 24 h were exposed to KA for 12 and 24 h (Fig. 3F). In the pUC-EP group, KA significantly induced the proliferation of BV2 cells. However, ABCG2 overexpression counteracted the KA-induced proliferation (Figs. S3C and D). Moreover, in pUC-EP cells, KA administration for 12 and 24 h significantly increased the ROS content and membrane distribution of Annexin V. However, overexpression of ABCG2 offset ROS overloading (Fig. 3G and H) and apoptosis (Fig. 3I and J), suggesting that overexpression of ABCG2 also benefited microglia to some extent.

3.4. Inhibition of ABCG2 activation by Ko143 abolished the protective effect of ABCG2 in neurons and microglia

We applied an inhibitor of ABCG2 (Ko143, 500 nM) [25] to ABCG2-transfected HT22 and BV2 cells to check the role of ABCG2 (Fig. 4A). The results demonstrated that 500 nM Ko143 did not affect the survival rate of HT22 cells (Fig. S3E) but reversed the protective effect of ABCG2 by increasing the ROS, membrane distribution of annexin V, and ferric ion content in neurons (Fig. 4B–D). Additionally, by inducing ROS and apoptosis in BV2 cells (Fig. 4E and F), we confirmed that overexpression of ABCG2 prevented glutamate- and KA-induced

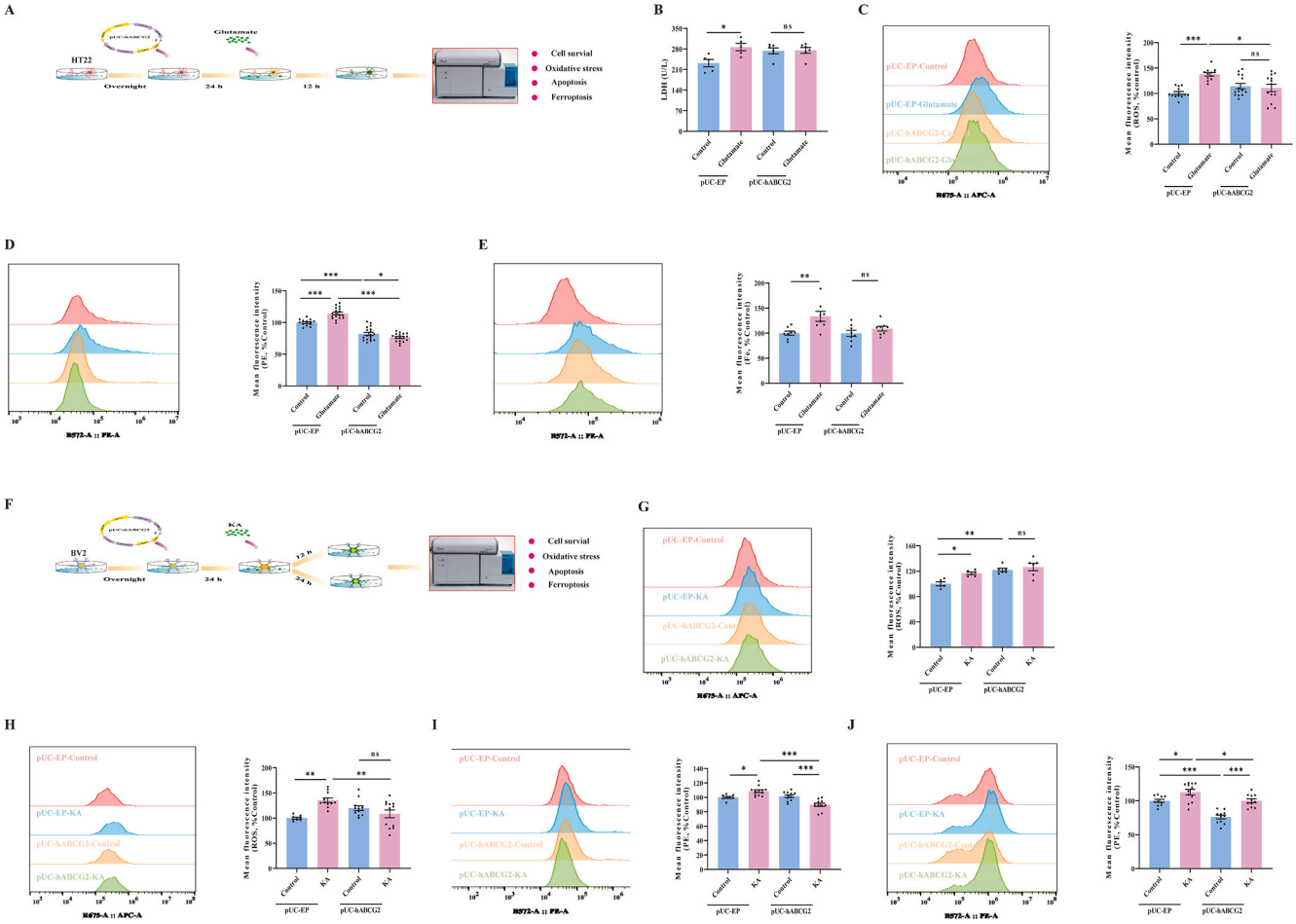

Fig. 3. Overexpression of ABCG2 prevented neurons from glutamate-induced injury. **(A)** Procedure of HT22 treated with ABCG2-plasmid. **(B)** LDH release of ABCG2 transfected cells treated with glutamate (pUC-EP groups, $n = 5$; pUC-hABCG2 groups, $n = 6$). **(C)** ROS content of ABCG2 transfected cells treated with glutamate ($n = 13$ per group). **(D)** Annexin V-PE fluorescent (Control of pUC-EP group, $n = 14$; glutamate of pUC-EP group, $n = 18$; pUC-hABCG2 groups, $n = 17$). **(E)** Ferri ion content of ABCG2 transfected cells treated with glutamate ($n = 8$ per group). **(F)** Procedure of BV2 treated with ABCG2-plasmid. **(G-H)** ROS content of ABCG2 transfected BV2 treated with KA for 12 h (**G**, Control of pUC-EP group, $n = 5$; glutamate of pUC-EP group, $n = 6$; pUC-hABCG2 groups, $n = 6$) and 24 h (**H**, Control of pUC-EP group, $n = 8$; glutamate of pUC-EP group, $n = 11$; pUC-hABCG2 groups, $n = 12$). **(I-J)** Annexin V-PE fluorescent of ABCG2 transfected BV2 treated with KA for 12 h (**I**, Control of pUC-EP group, $n = 8$; glutamate of pUC-EP group, $n = 12$; pUC-hABCG2 groups, $n = 11$) and 24 h (**J**, Control of pUC-EP group, $n = 10$; glutamate of pUC-EP group, $n = 12$; pUC-hABCG2 groups, $n = 11$). Data are presented as means ± SEM. Results designated with ns were not significant, whereas those designated with * ($P < 0.05$), ** ($P < 0.01$), ***($P < 0.001$) were significant according to adjusted P values in each indicated comparison.

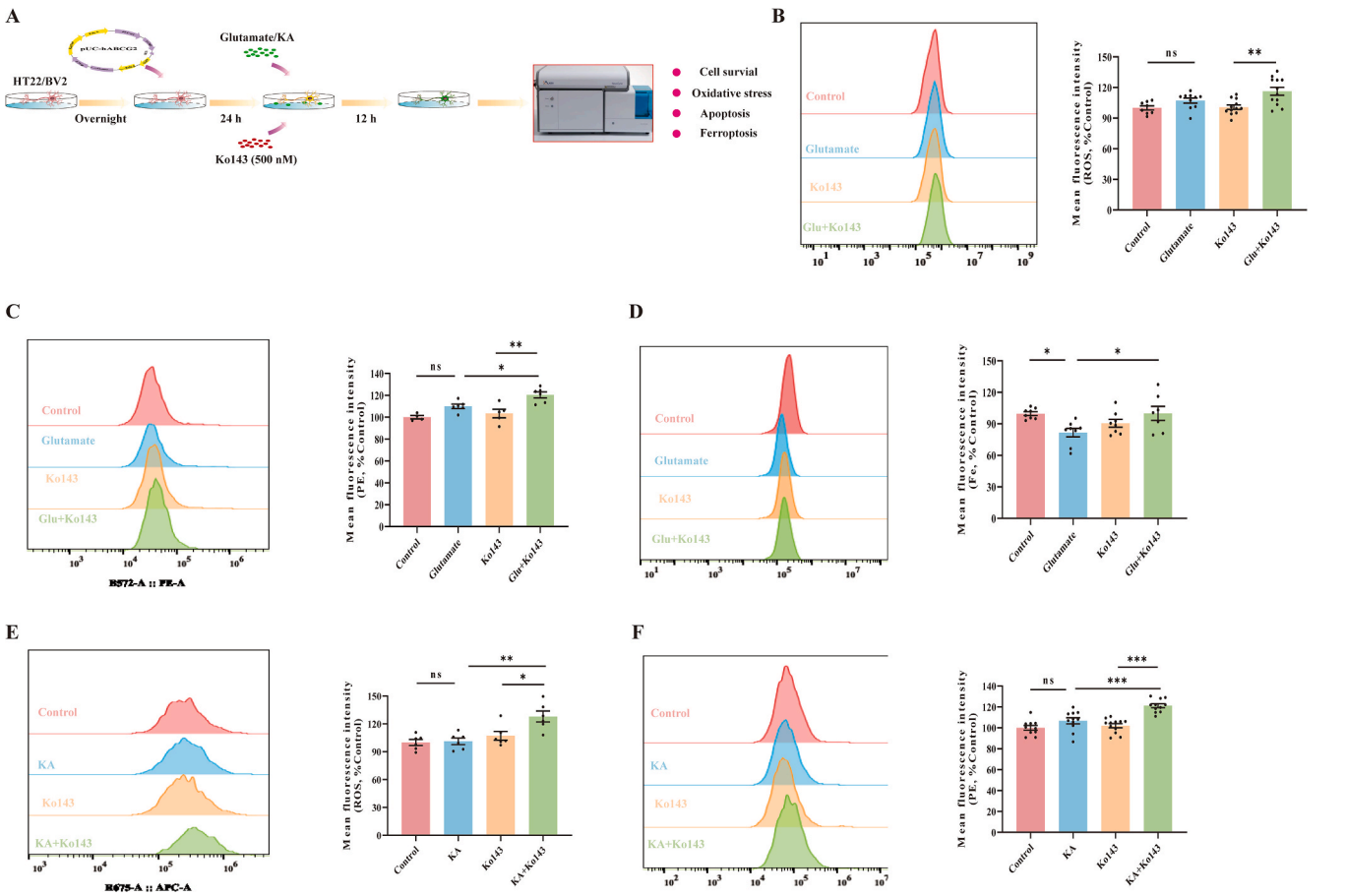

Fig. 4. Ko143 abolished the protective effect in ABCG2-overexpressed cells. **(A)** Procedure of ABCG2-overexpressed HT22 treated with ABCG2 inhibitor Ko143 and glutamate. **(B-D)** ROS content (**B**, $n = 8$, 10,12, 12, respectively), annexin V-PE fluorescent (**C**, $n = 4$, 6, 5, 6, respectively), and Ferri ion content (**D**, $n = 8$, 8, 8, 7, respectively) of ABCG2 transfected HT22 treated with Ko143 and glutamate for 12 h. **(E-F)** ROS content (**E**, $n = 6$ per group) and annexin V-PE (**F**, $n = 10$, 11, 12, 11, respectively) fluorescent of ABCG2 transfected BV2 treated with Ko143 and glutamate for 12 h. Data are presented as means ± SEM. Results designated with ns were not significant, whereas those designated with * ($P < 0.05$), ** ($P < 0.01$), ***($P < 0.001$) were significant according to adjusted P values in each indicated comparison.

excitotoxicity in neurons and microglia.

3.5. CRISPR-CAS9-generated knockout of ABCG2 shortened the survival time and decreased the survival rate of mice induced by acute seizure

We constructed a CRISPR-based knockout mice to further validate the role of ABCG2 in epilepsy (Fig. 5A). Deletion of ABCG2 was confirmed using qPCR, and a significant decrease in *ABCG2* mRNA expression was found in the ABCG2$^{-/-}$ mice compared to the WT mice (Fig. 5B). The ABCG2$^{-/-}$ mice showed normal body weight from four to nine weeks compared to the WT mice, except at six-weeks of age (Fig. 5C). Significantly decreased central distance in the open field test in the 6th week and increased fecal counts in the 8th weeks were observed in ABCG2$^{-/-}$ mice compared with WT mice, but not in the other weeks (Fig. 5D–G), suggesting that abolition of ABCG2 limited the effect on cognitive function. However, when ABCG2$^{-/-}$ mice were administered 90 mg/kg (i.p.) of PTZ, no effect on the latent period and seizure counts of episodes with scores of 2–5 were obsereved (Fig. 5H and I) but significantly shorter survival time and decreased survival rate were found compared with WT mice (Fig. 5J and K), suggesting that ABCG2 deficiency did not cause seizure susceptibility but augmented seizure-related death.

3.6. Label-free proteomics analysis identified the molecular mechanisms of ABCG2-deficiency

We performed a DIA-free proteomic analysis of the hippocampi of ABCG2$^{-/-}$ and WT mice after treatment with PTZ to explore the molecular mechanisms underlying ABCG2 effects (Fig. 6A). In total, 39,102 peptides were identified, of which 37,121 were unique. A total of 5112 proteins were confirmed by DIA-NN, of which 133 showed significant changes between ABCG2$^{-/-}$ and WT mice (fold change >1.2 or < 0.833, $P < 0.05$; Fig. 6B). While, 53 differentiated expression proteins (DEPs) including ABCG2, RNA binding motif protein 41 (Rbm41), G protein-coupled receptor kinase 5 (Grk5), and DDRGK domain containing protein 1 (Ddrgk1) were significantly decreased in the ABCG2$^{-/-}$ mice and 70 DEPs such as Ig heavy chain V, ASH1 like histone lysine methyltransferase (Ash1l), T-cell specific GTPase 2 (Tgtp2), indolethylamine *N*-methyltransferase (Inmt), guanylate binding protein (Gbp) 4 were increased, compared with WT mice (Fig. 6C). The deficiency of the unique peptide ABCG2 (TIIFSIHQPR) was further examined (Fig. 6D). Pathway and GO enrichment analyses by GSEA demonstrated that complementary and coagulation-related cascades, staphylococcus aureus infection, carbon metabolism, valine, leucine, and isoleucine degradation, and ECM-receptor interaction were the most enriched pathways with upregulated DEPs (Fig. 6E), while the functions of regulation of acute inflammatory response, regulation of protein maturation, immunoglobulin-mediated immune response, cellular responses to interferon-beta, blood coagulation, and fibrin clot formation were

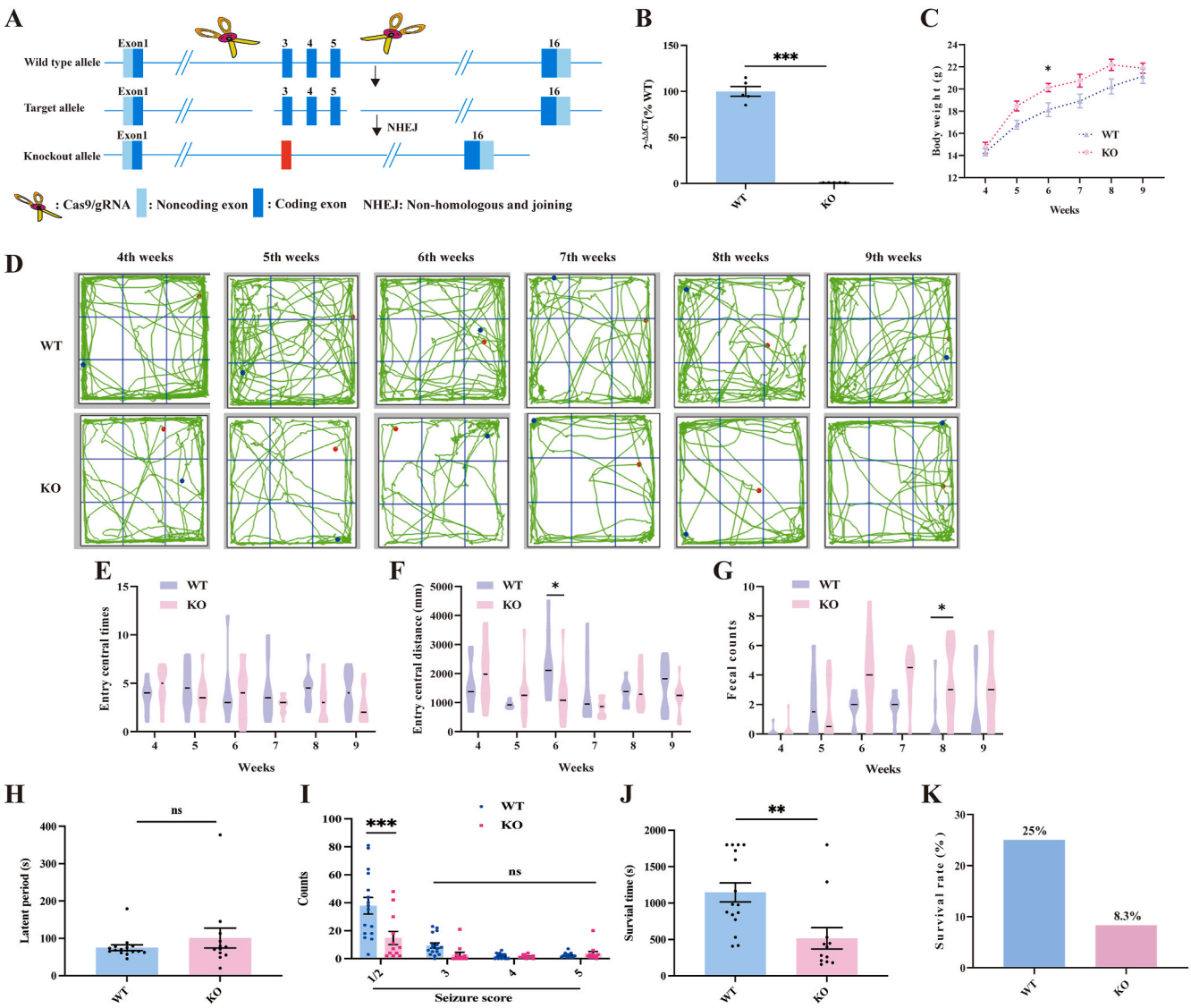

Fig. 5. CRISPR-CAS9 knockout ABCG2 shortened the survival time and decreased the survival rate of mice induced by acute PTZ. **(A)** CRISPR-CAS strategy of knocking out ABCG2 in C57BL/6J mice. **(B)** mRNA expression of *ABCG2* in the hippocampi of wildtype (WT) and ABCG2 $^{-/-}$ (KO) mice ($n = 5$ per group). **(C)** Body weight of wild type and ABCG2 KO mice from 4 to 9 weeks ($n = 12$ per group). **(D)** Present figures of the open-field test. **(E)** Entry central time (WT groups, $n = 8$; KO groups, $n = 12$). **(F)** Entry central distance (WT groups, $n = 8$; KO groups, $n = 12$). **(G)** Fecal counts (WT groups, $n = 8$; KO groups, $n = 12$). **(H)** Latent period of wildtype and ABCG2 KO mice administered by PTZ at 9th week (WT, $n = 16$; KO: $n = 12$). **(I)** Seizure counts of 1/2, 3, 4, and 5 score (WT, $n = 16$; KO, $n = 12$). **(J)** Survival time of WT and ABCG2 KO mice since treating with PTZ (WT, $n = 16$; KO, $n = 12$). **(K)** Survival rate (WT, $n = 16$; KO, $n = 12$). Data are presented as means ± SEM. Results designated with ns were not significant, whereas those designated with * ($P < 0.05$), ** ($P < 0.01$), ***($P < 0.001$) were significant according to adjusted P values in each indicated comparison.

involved in ABCG2 deficit-induced damage (Fig. 6F). Among them, the cellular response to interferon-beta showed the most DEPs, including Tgtp2, Gbp4, interferon-induced protein with tetratricopeptide repeats 1 (Ifit1), Gbp2, signal transducer and activator of transcription 1 (STAT1), and immunity-related GTPase family M membrane 1 (Irgm1) (Fig. 6G). STAT1 was the core protein extracted from STRING analysis (Fig. 6H), suggesting that STAT1 plays a vital role in the protection of ABCG2.

3.7. STAT1 and mTOR are involved in the prevention effect of ABCG2 independent by JAK1 and AKT

STAT1 is a core protein that regulates interferon-mediated effects [26]. We assessed the RNA and protein content in ABCG2$^{-/-}$ and WT mice to investigate whether the knockout of ABCG2 affected the background expression of STAT1. The results demonstrated that ABCG2 deficiency did not disrupt mRNA, total STAT1, or phosphorylation levels of STAT1 in the hippocampi (Figs. S4A and B). ABCG2$^{-/-}$ mice treated with PTZ showed remarkably increased *STAT1* mRNA expression and protein expression of STAT1β, which is a *C*-terminal-truncated 84-KD version of STAT1 lacking S727 but including Y701 [27]; however, no changes in the phosphorylation of STAT1 at Y701 were observed between ABCG2$^{-/-}$ and WT mice (Fig. 7A–C). The Janus kinase 1 (JAK1)-STAT1 pathway is the major pathway mediating interferon-γ action. Once interferon-γ targets the interferon production regulator (IFNR), JAK1 is activated, which induces the phosphorylation of STAT1 [28]. However, the protein expression and phosphorylation levels of JAK1 were not in parallel with those of STAT1 in the PTZ-treated ABCG2$^{-/-}$ mice (Fig. 7D), suggesting that the role of STAT1 was independent of JAK1.

Since the mammalian target of rapamycin kinase (mTOR) deletion impairs the activation and proliferation of microglia, exacerbates the

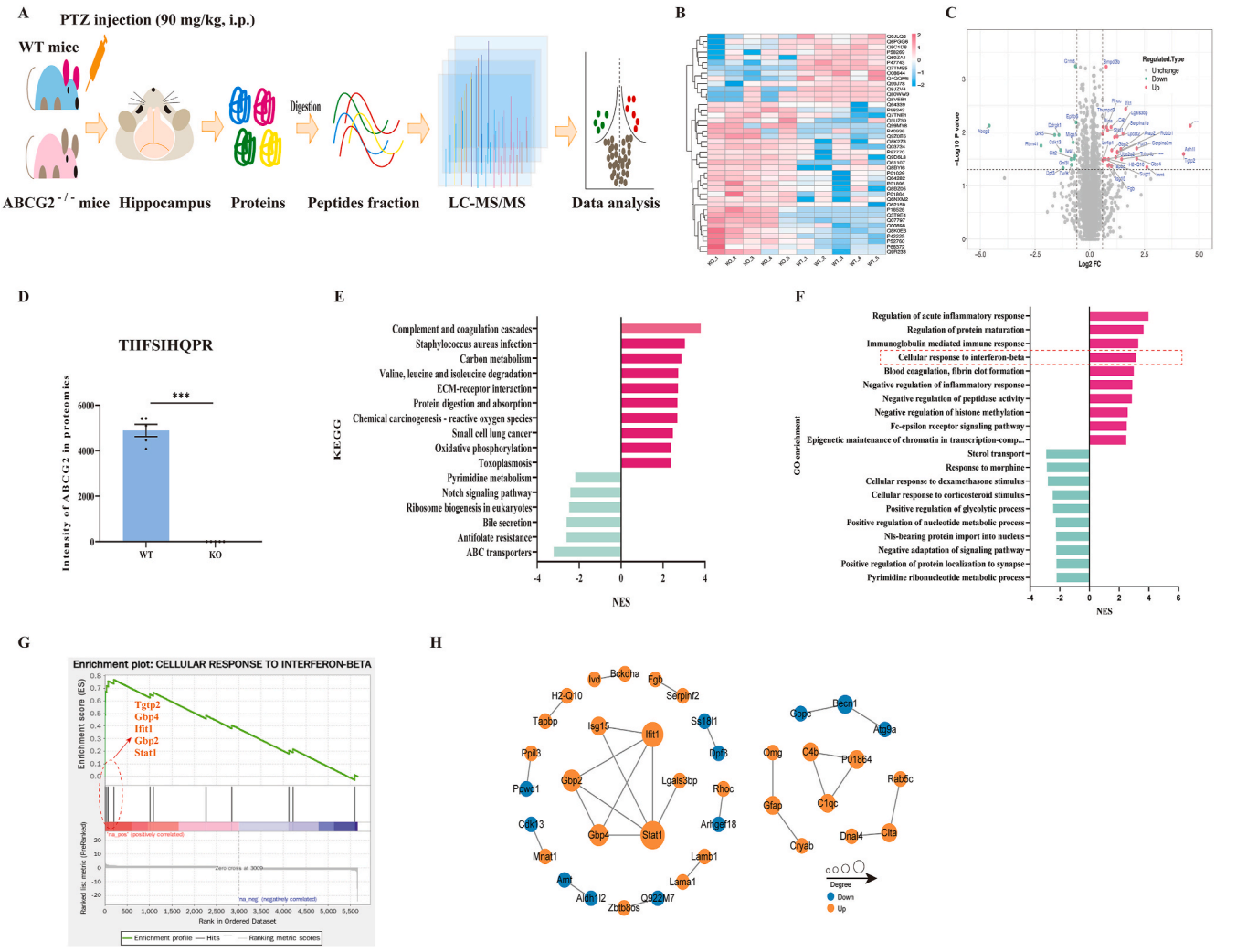

Fig. 6. Comparison of proteomics of hippocampi between WT and ABCG2 KO mice administered by PTZ. **(A)** Schematic procedure of hippocampi proteomics analysis (WT, $n = 5$; KO, $n = 5$). **(B)** Heatmap for 133 differentiated expression proteins (DEPs). **(C)** Volcano plot of 133 DEPs. **(D)** Peptide intensity of ABCG2 between WT and KO mice. **(E)** Pathway analysis of 133 DEPs. **(F)** Gene Ontology enrichment of 133 DEPs. **(G)** GSEA analysis of cellular response to interferon-beta. **(H)** Core proteins of total DEPs. Data are presented as means ± SEM. Results designated with ***($P < 0.001$) were significant values.

loss of neurons, and promotes epileptogenesis [29], which also positively regulates STAT1 [30], we explored the phosphorylation level of the serine/threonine kinase (AKT)-mTOR pathway. PTZ-treated ABCG2$^{-/-}$ mice showed a significant decrease in the phosphorylation of mTOR, but not in the total AKT expression and phosphorylation of AKT (Fig. 7E–G), illustrating the independent effect of mTOR in ABCG2$^{-/-}$ mice. Moreover, depending on the regulation of protein maturation (Fig. 6F), we also detected the expression of the endoplasmic reticulum stress-associated protein C/EBP-homologous protein (CHOP) and found that ABCG2$^{-/-}$ mice treated with PTZ showed a significant increase in CHOP (Fig. 7H).

We further examined the protein expression levels of mTOR and CHOP in ABCG2-overexpressed HT22 cells. In pUC-EP cells, glutamate treatment induced a decrease in the expression of *p*-mTOR/mTOR and an increase in the expression of CHOP. However, cells transferred by ABCG2-containing plasmid counteracted the effect of glutamate (Fig. 7I–K). Furthermore, interruption of the mTOR inhibitor rapamycin (RAPA), which was confirmed by decreased phosphorylation of mTOR, reversed the protective effect against apoptosis in ABCG2-overexpressing HT22 (Fig. 7L-N), suggesting that the mTOR pathway is involved in the preventive effect of ABCG2. However, inhibition of mTOR did not affect total STAT1 levels or its phosphorylation (Fig. 7O-P), which illustrated that the role of STAT1 in ABCG2 was also independent of mTOR.

3.8. ABCG2 is directly bound to STAT1 and mTOR

We suspected a direct interaction between ABCG2, mTOR, and STAT1 because mTOR and STAT1 are regulated independently. Therefore, we performed COIP in HT22 cells treated with or without glutamate, and the results demonstrated that ABCG2 bound to STAT1 and mTOR, whereas glutamate-induced HT22 cells showed an increasing interaction (Fig. 8A–C). Furthermore, using immunofluorescence, mTOR or STAT1 showed apparent colocalization with ABCG2 in the cytoplasm and nucleus of glutamate-treated HT22 cells (Fig. 8D), suggesting that instant overexpression of ABCG2 contacted mTOR and STAT1.

3.9. Deficiency of ABCG2-induced ISGylation of STAT1 and mTOR to accumulate STAT1 and inhibit mTOR phosphorylation

The protein expression of STAT1 in PTZ-treated ABCG2$^{-/-}$ mice was significantly increased, but there was no change in phosphorylation at the Y701 site, which indicated that the phosphorylation of STAT1 was impeded. Previous studies have demonstrated that SUMOylation of STAT1 at K703 inhibits the phosphorylation of Y701 [31,32].

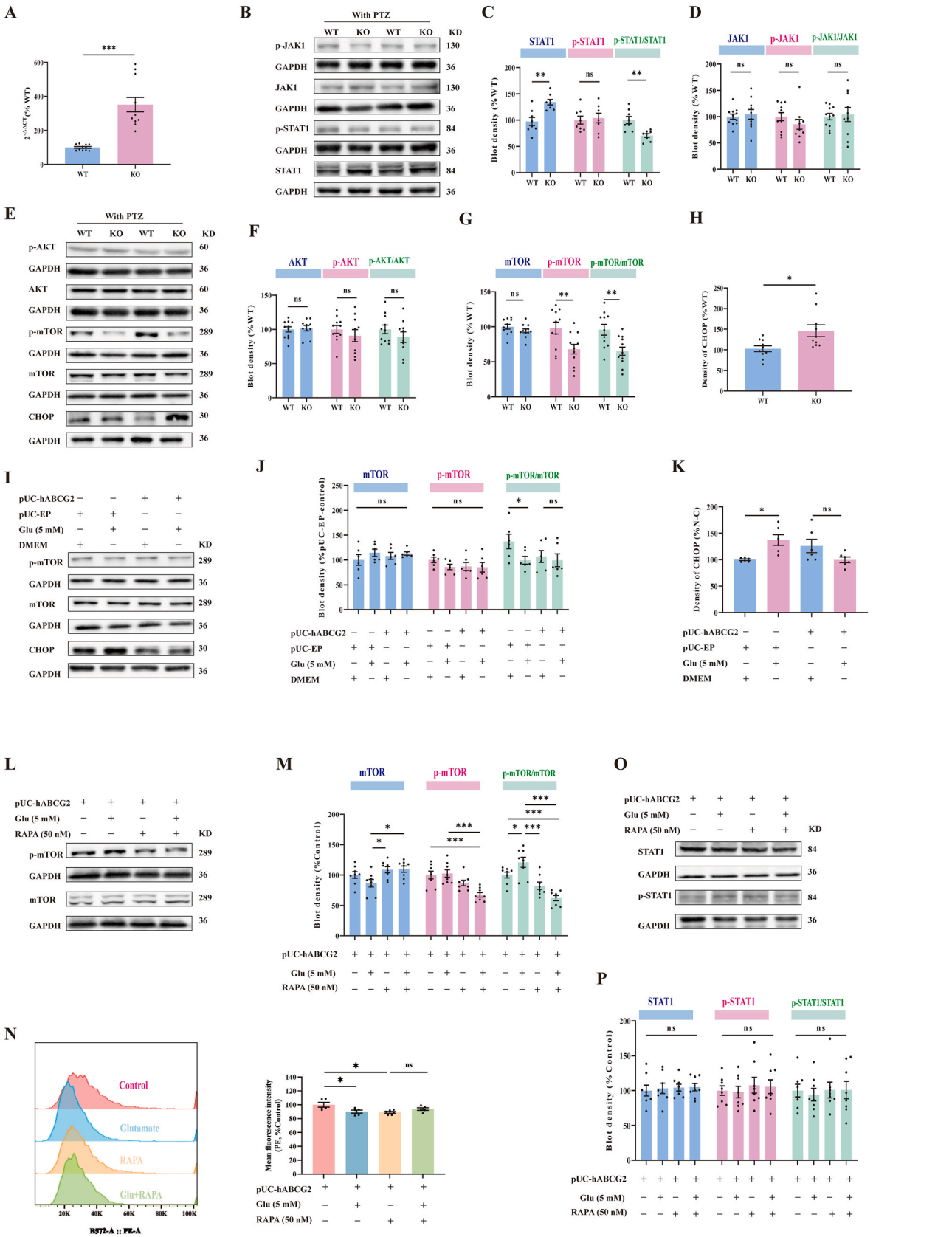

(caption on next page)

Fig. 7. STAT1 and mTOR involved in the protective effect of ABCG2. (**A**) mRNA expression of *STAT1* in the hippocampi of ABCG2 $^{-/-}$ mice and WT mice administered by PTZ ($n = 11$ per group). (**B-D**) Representative images (**B**) and quantification by densitometry of Western blot analysis of STAT1 (**C**, $n = 8$ per group) and JAK1 (**D**, WT, $n = 11$; KO, $n = 10$) in the total protein extracted from the hippocampi of ABCG2 $^{-/-}$ mice and WT mice. (**E-H**) Representative images (**E**) and quantification by densitometry of Western blot analysis of AKT (**F**, WT, $n = 11$; KO, $n = 10$), mTOR (**G**, WT, $n = 11$; KO, $n = 12$), and CHOP (**H**, $n = 7$ per group) in the total protein extracted from the hippocampi of ABCG2 $^{-/-}$ mice and WT mice. (**I–K**) Representative images (**I**) and quantification by densitometry of Western blot analysis of mTOR (**J**, $n = 6$ per group) and CHOP (**K**, $n = 6$ per group) in the total protein extracted from transfected HT22 cells with or without glutamate. (**L-M**) Representative images (**L**) and quantification by densitometry of Western blot analysis of mTOR (**M**, $n = 8$ per group) in the total protein extracted from transfected HT22 cells with or without glutamate and rapamycin. (**N**) Representative images and quantification of annexin V-PE in transfected HT22 cells with or without glutamate and rapamycin by using fluorescent flow cytometry ($n = 5$ per group). (***O–P***) Representative images (**O**) and quantification by densitometry of Western blot analysis of STAT1 (**P**, $n = 8$ per group) in the total protein extracted from transfected HT22 cells with or without glutamate and rapamycin. Data are presented as means ± SEM. Results designated with ns were not significant, whereas those designated with * ($P < 0.05$), ** ($P < 0.01$), ***($P < 0.001$) were significant according to adjusted *P* values in each indicated comparison.

Previously, our proteomic data showed that the protein expression of interferon-stimulated gene 15 (ISG15), which can ISGylate STAT1 [33] and mTOR on lysine 2066 [34], was significantly higher in ABCG2$^{-/-}$ mice than that in WT mice (Fig. 6C). Therefore, we suspected that ISG15 or ISGylation affects the accumulation of STAT1 and phosphorylation of mTOR. Hence, we first examined the RNA and protein expression levels of ISG15 and ISGylation in ABCG2$^{-/-}$ and WT mice treated with PTZ. ABCG2$^{-/-}$ mice showed a significant increase *ISG15* RNA expression and ISGylation but not in free ISG15 protein levels (Fig. 9A–C). After performing COIP by using ABCG2, STAT1 and mTOR antibodies, we determined that in the precipitation complex, STAT1 and mTOR but not ABCG2 were apparently ISGylated in the HT22 cells treated with or without glutamate (Fig. 9D–F). Furthermore, STAT1 and mTOR were ISGylated in the cortex of ABCG2$^{-/-}$ mice treated with PTZ compared to that in WT mice (Fig. 9G and H), suggesting that ABCG2 deficiency induces ISGylation, resulting in the accumulation of STAT1 and inhibition of mTOR phosphorylation.

3.10. Overexpression of transcription factor hypoxia-inducible factor1 (HIF-1)α in glutamate-induced neuronal injury and KA- and LPS-induced inflammation of BV2 cells

A previous study revealed that the transcription factor HIF-1α is involved in hypo-oxidation, is associated with epilepsy, and binds to the ABCG2 promoter [35,36]. However, the regulation effects of HIF-1α on ABCG2 during epileptogenesis remain unknown. Therefore, we detected the protein expression of HIF-1α. Neuronal cells treated with 1 and 5 mM glutamate for 12 h showed significantly increased HIF-1α protein expression. Moreover, an increasing tendency emerged at 12 and 24 h and smoothly decreased to normal levels from 48 to 96 h (Fig. 10A and B). Similarly, the administration of KA for 12 or 24 h also increased the protein expression of HIF-1α (Fig. 10C). Those phenomena were found in the LPS- and KA-induced microglia with increased HIF-1α expression (Fig. 10D and E). Fluorescence images showed that in cells induced by KA for 12 and 24 h, overexpressed HIF-1α, were colocalized with the ABCG2 protein (Fig. 10F) and illustrated the correlation between HIF-1α and ABCG2. These results make us speculate whether ABCG2 was regulated by HIF1α as a stimulator. Therefore, we constructed a shRNA plasmid of HIF-1α to knock down its protein expression in HT22 (Fig. 10G). Intriguingly, the knockdown of HIF1α led to a significant reduction in ABCG2 expression caused by glutamate (Fig. 10H), indicating that induced expression of ABCG2 may be regulated by HIF1α.

4. Discussion

ABCG2 is a medically important ATP-binding cassette transporter known for its role in the transport of chemically diverse toxins and drugs. In the nervous system, the overexpression of ABCG2 in the BBB limits brain penetration and restricts exposure to drugs such as abemaciclib and olaparib [37,38]. Moreover, ABCG2 is overexpressed in neurological disorders such as Alzheimer's disease [39], glioblastomas [40], and amyotrophic lateral sclerosis [41]. However, studies on the expression of ABCG2 in epileptogenesis show contradictory results [39,42], and its role in epilepsy remains uncertain. In this study, we found that the mRNA and protein expression of ABCG2 were significantly increased in the hippocampi of rats under PTZ-induced acute (60 mg/kg, i.p.) and chronic (35 mg/kg, i.p.) seizure conditions (Fig. 1B–H). This observation is consistent with the results of a study by Harby and colleagues that showed a significan increase in the protein expression of ABCG2 with 50 mg/kg of PTZ [7]. Using KA, which stimulates glutamate to induce chronic epilepsy to mimic human temporal lobe epilepsy, we also observed a gradual increase in ABCG2 levels from the first day of injection, peaked on the 7th day and dropped down on the 30th day (Fig. 1I-N). This temporal pattern correlated with locomotor activity in the open-field test and aligns with the reported peak brain injury period of 7 days post-SE in C57BL/6J mice [43]. Our results illustrate that epilepsy induces the overexpression of ABCG2 in response to various stimuli across species, including rats and mice. Furthermore, we revealed that this increased ABCG2 expression was localized in neurons and microglia. We next confirmed *in vitro* that ABCG2 overexpression was activated in mouse neuronal cell (HT22) treated with glutamate and KA, as well as in the microglia cells (BV2) stimulated by KA and LPS. This observation illustrates that the overexpression of ABCG2 may act as an effector in these cells when stimulated by glutamate, KA, and the inflammatory factor LPS. However, this observation contrasts with the study by Gibson et al. [44], which reported that the administration of 1–500 ng/mL of LPS for 24 h decreased ABCG2 expression of both mRNA and protein in BV2 cells. These differences were likely due to the discrepancy in LPS concentrations between the two studies. Previous research indicates that lower concentrations of pro-inflammatory cytokines (IL-1B, TNF-a, and IL-6) and glutamate (below 100 μM) do not induce the mRNA and protein expression of ABCG2 in the BBB [45], hCMEC/D3 human endothelial cells [46], and human brain capillaries [47]. Consistent with previous studies, we used concentrations of glutamate, LPS, and KA that are pathologically relevant to epileptogenesis [48,49]. In conclusion, our study shows that epilepsy induces an increase in ABCG2 expression.

In this study, we demonstrated that ABCG2 overexpression may offset the cytotoxicity of glutamate by improving ROS overload, annexin V protein ectropion, and iron overload. Ko143, an ABCG2 inhibitor, reversed these protective effects, illustrating the preventive role of ABCG2. This result is in accordance with previous studies reporting the significance of ABCG2 as a toxic and drug efflux transmembrane protein, thus preventing cells from toxic agent-mediated damage *in vitro* [50,51]. Furthermore, our *in-vivo* analysis confirmed that ABCG2 acts as a shield against epilepsy. ABCG2 $^{-/-}$ mice treated with 90 mg/kg of PTZ showed significantly shortened survival time and decreased survival rate compared to WT mice (Fig. 7J and K). This observation illustrates that the loss of function of ABCG2 exacerbated seizures, which is in accordance with previous studies showing that ABCG2 deficiency augments oxidative stress in transgenic AD mice [52] and indicating that ABCG2 acts as a surviving factor for plasma cells that can relieve the endoplasmic reticulum [53].

STAT1 is a major transcription factor in the IFN-α/β IFN-γ signal-transduction pathway, which is closely associated with epilepsy. Elevated STAT1 protein expression in the CA1 KA-induced and

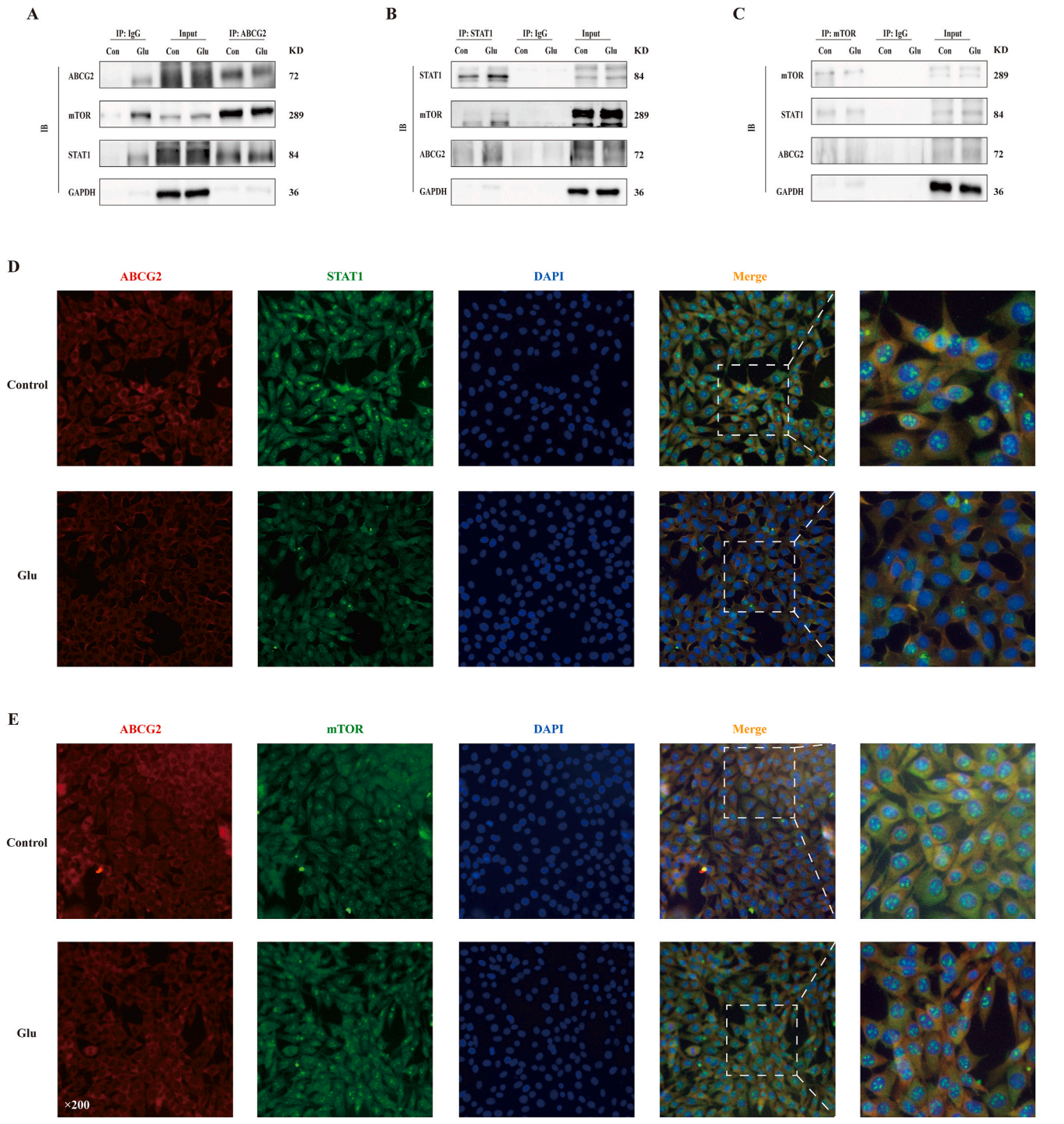

Fig. 8. Directly combination among ABCG2, STAT1, and mTOR. **(A-C)** Representative western blots of lysates and COIP for ABCG2 (**A**), STAT1 (**B**), and mTOR (**C**) in the HT22 cells treated with or without glutamate, $n = 3$ per experiment. **(D)** Representative colocalization images of ABCG2 (Red), STAT1 (Green), and DAPI (Blue) in the HT22 cells treated with or without glutamate ($n = 3$ per group). **(E)** Representative colocalization images of ABCG2 (Red), mTOR (Green), and DAPI (Blue) in the HT22 cells treated with or without glutamate ($n = 3$ per group). (For interpretation of the references to colour in this figure legend, the reader is referred to the Web version of this article.)

electrical-kindling rats has been previously demonstrated [54,55]. Two main statuses of STAT1 contribute towards regulation of the IFN signaling pathway. Tyrosine phosphorylation of STAT1 at position 701 induces homodimerization, nuclear translocation, and binding to the elements of IFN-induced genes. In contrast, unphosphorylated STAT1 acts as a dimer and monomer to induce IFN-associated genes such as LMP2 and IFIT1 [56,57]. Using proteomics, we confirmed that STAT1 was the core differentially expressed protein that was significantly increased in ABCG2 $^{-/-}$ mice administered PTZ in parallel with other IFN-stimulating proteins, including IFIT1 and ISG15. However, no change in phosphorylation and dimerization of STAT1 (Fig. S4E) was observed, which suggested that accumutaion of the monomer STAT1 may be a potential effector for PTZ. ISG15 is an IFN-a/B-inducible, ubiquitin-like protein that can be conjugated to approximately 400 intracellular substrate proteins via ISGylation. ISG15 and ISGylation reportedly increase protein stability and interfere with the

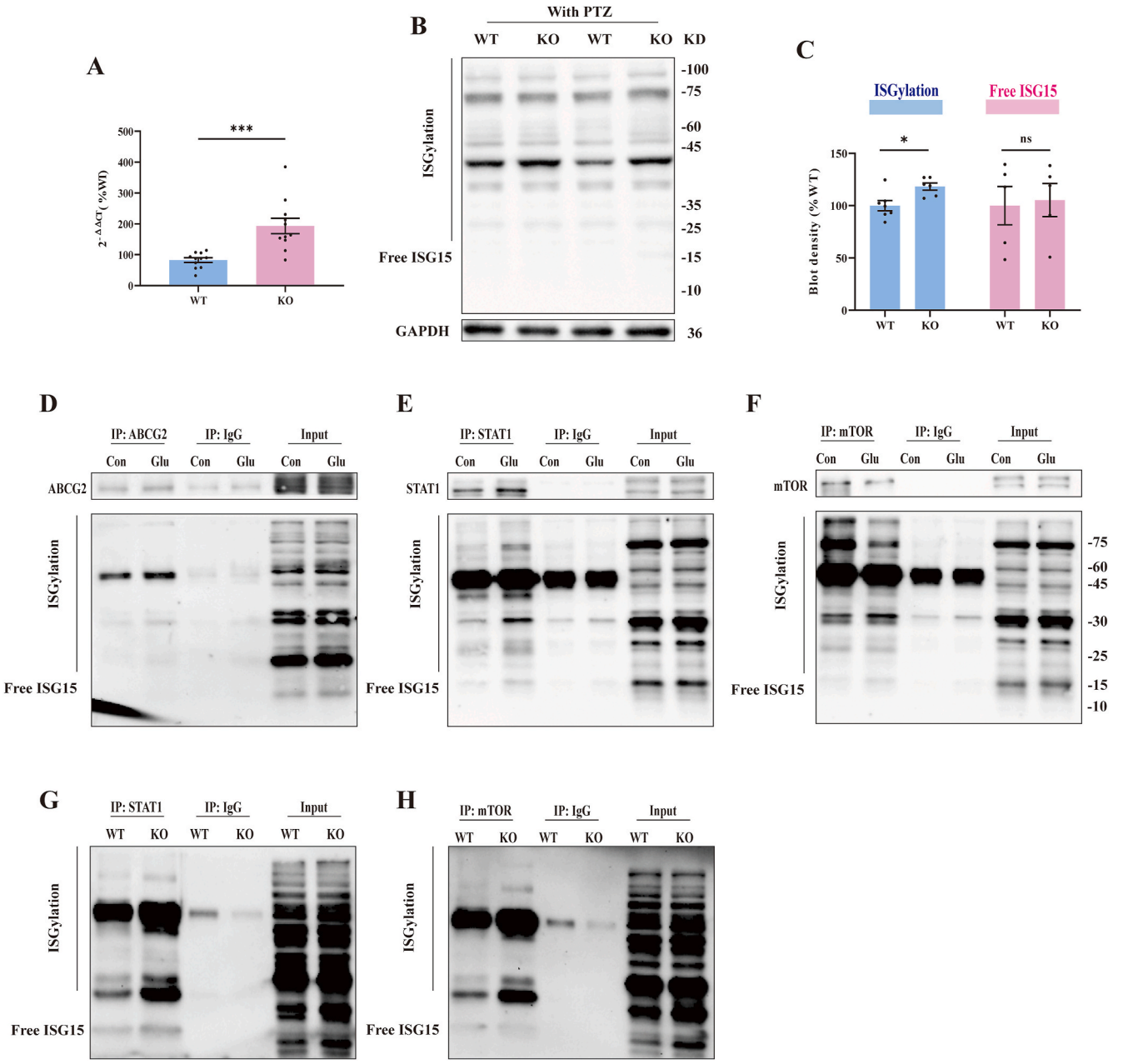

Fig. 9. Deficiency of ABCG2 induced accumulation of STAT1 and inhibited the phosphorylation of mTOR via ISGylation. **(A)** mRNA expression of *ISG15* in the hippocampi of ABCG2 $^{-/-}$ mice and WT mice administered by PTZ ($n = 11$ per group). **(B–C)** Representative images (**B**) and quantification by densitometry of Western blot analysis of free-ISG15 ($n = 5$ per group) and ISGylation (**C**, WT, $n = 7$; KO, $n = 6$) in the total protein extracted from the hippocampi of ABCG2 $^{-/-}$ mice and WT mice. **(D-F)** Representative western blots of lysates and COIP for ISGylation of ABCG2 (**D**), STAT1 (**E**), and mTOR (**F**) in the HT22 cells treated with or without glutamate ($n = 3$ per group). **(G-H)** Representative western blots of lysates and COIP for ISGylation of STAT1 (**G**) and mTOR (**H**) in the cortex of ABCG2 $^{-/-}$ mice and WT mice treated with PTZ ($n = 4$ per group). Data are presented as means ± SEM. Results designated with ns were not significant, whereas those designated with * ($P < 0.05$) and *** ($P < 0.001$) were significant according to adjusted P values in each indicated comparison.

ubiquitination and degradation of proteins such as YAP, USP18, and STAT1 [58–60]. In this study, we demonstrated increased levels of ISGylation in ABCG2 $^{-/-}$ mice stimulated by PTZ compared to WT mice and ISGylation of STAT1 in glutamate-induced neurons, suspecting that in the ABCG2 $^{-/-}$ mice, ISGylation of STAT1 ensured protein stabilization, resulting in the accumulation of ABCG2 and induction of neuronal apoptosis.

Although JAK1-STAT1 is the main pathway regulating IFN [28] and the AKT-mTOR-STAT1 pathway is correlated with excitatory injury, we did not find significant expression of JAK1 and AKT between ABCG2 $^{-/-}$ and WT mice, except for mTOR. mTOR is a central controller of cell growth, proliferation, and survival [61]. Microglial mTOR deletion impairs the activation and proliferation of microglia, destroys microglial phagocytosis, exacerbates neuronal loss, and promotes epileptogenesis [29]. mTOR inactivation induces neuronal ROS overload and cell death [62]. In this study, we demonstrated the inactivation of mTOR in ABCG2 $^{-/-}$ mice and in glutamate-induced neurons. However, overexpression of ABCG2 increased the phosphorylation level of mTOR, while further use of rapamycin, an inhibitor of mTORC1, offset the protective effect of ABCG2, suggesting that the protective effect of ABCG2 is regulated by activation of mTOR, which agrees with Smith's study showing that activation of mTOR increased neuronal survival [63]. In ABCG2 $^{-/-}$ mice, we demonstrated increased ISGylation of mTOR, which is in agreement with a previous study showing that mTOR was ISGylated on

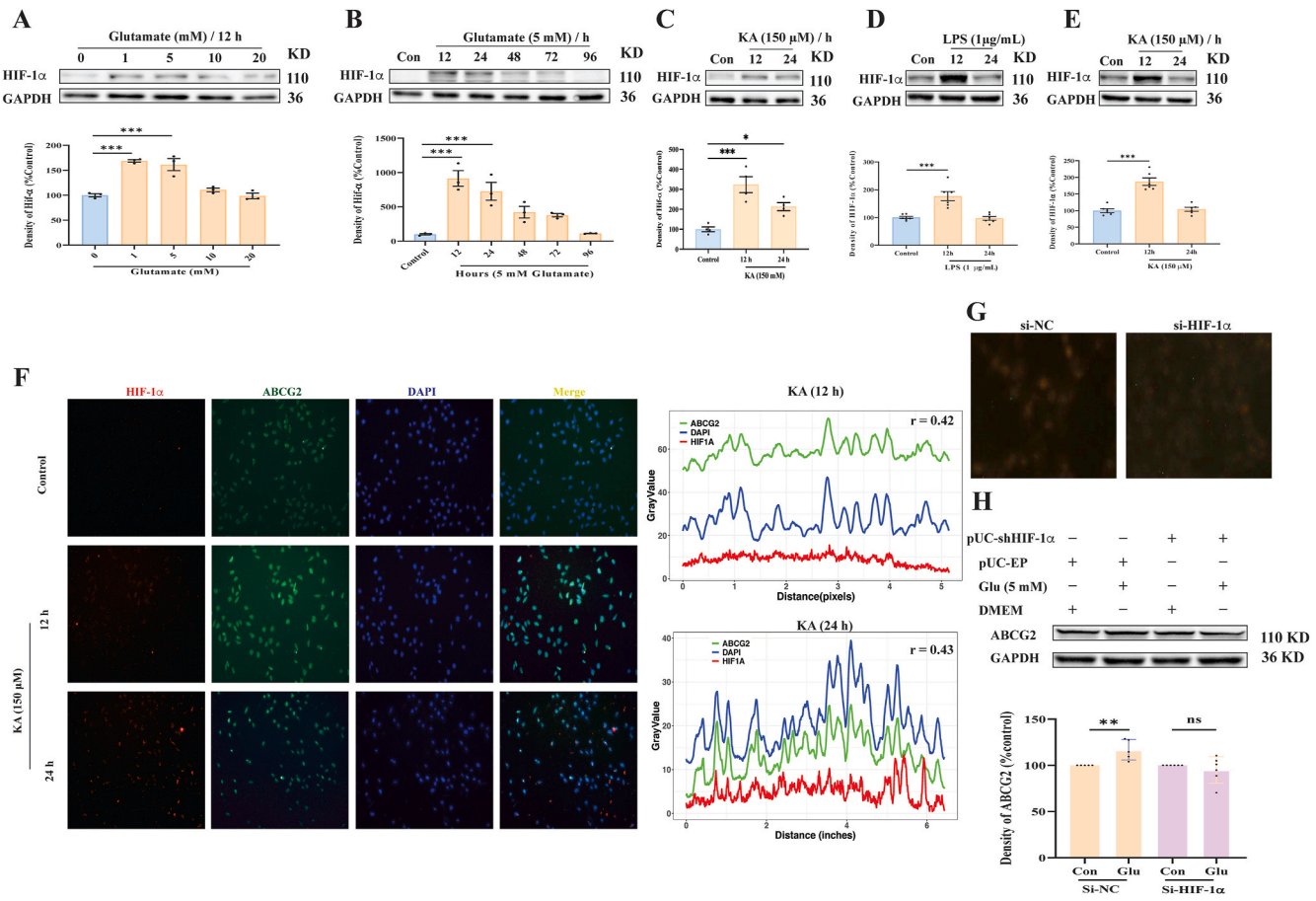

Fig. 10. Overexpression of transcript factor HIF-1α in glutamate-induced neuron injury and KA and LPS-induced BV2 inflammation. **(A)** Protein expression of HIF-1α in HT22 treated with 1, 5, 10, and 20 mM of glutamate for 12 h ($n = 3$ per group). **(B)** Protein expression of HIF-1α in HT22 treated with 5 mM of glutamate for 12, 24, 48, 72, and 96 h ($n = 3$ per group). **(C)** Protein expression of HIF-1α in HT22 treated with 150 μM of KA for 12 and 24 h ($n = 4$ per group). **(D-E)** Protein expression of HIF-1α in BV2 treated with 1 μg/mL of LPS for 12 and 24 h (**D**, $n = 6$ per group) or 150 μM of KA for 12 h and 24 h (**E**, $n = 6$ per group). **(F)** Representative colocalization images of HIF-1α (Red), ABCG2 (Green), and DAPI (Blue) in the HT22 cells treated with or without KA for 12 and 24 h. **(G)** Representative graphs of HT22 cells transfected with empty plasmid or sh–HIF–1α plasmid ($n = 3$ per group). **(H)** Representative images and quantification by densitometry of Western blot analysis of ABCG2 in the total protein extracted from sh–HIF–1α-transfected HT22 cells with or without glutamate ($n = 5$ per group). Data are presented as means ± SEM. Results designated with ns were not significant, whereas those designated with * ($P < 0.05$), ** ($P < 0.01$), ***($P < 0.001$) were significant according to adjusted P values in each indicated comparison. (For interpretation of the references to colour in this figure legend, the reader is referred to the Web version of this article.)

its lysine 2066 residue [34], suggesting that ISGylation of mTOR may interfere with its phosphorylation. However, we did not observe any inference of total STAT1 or phosphorylation of STAT1 by rapamycin, which further confirmed the direct interaction between ABCG2, mTOR, and STAT1 in neurons to form a complex. Therefore, we suspected that the overexpression of ABCG2 tended to recruit STAT1 and mTOR, decrease the cytoplasmic effect of STAT1, and induce mTOR phosphorylation to prevent neuronal apoptosis. After the deletion of ABCG2, the complex of ABCG2, mTOR, and STAT1 was separated, leading to the induction of mTOR and STAT1 independently in the cytoplasm; this makes mTOR and STAT1 susceptible to ISGylation, resulting in mTOR inactivation and STAT1 accumulation to promote neuronal apoptosis.

This study identified an instant increase in ABCG2, which acts as a shield in epileptogenesis, relieves oxidative stress and apoptosis of neurons and microglia, and is closely related to the ISGylation of STAT1 and mTOR, revealing a potential target to relieve epilepsy.

Funding information

This study was supported by the Hainan Provincial Key Research and Development Program (ZDYF2021SHFZ092 and ZDYF2022SHFZ109), National Natural Science Foundation of China (No. 82360838), Epilepsy Research Science Innovation Group of Hainan Medical University (2022), Hainan Province Clinical Medical Center (2021), Innovation and Entrepreneurship Training Program for College Students (No. 11810123), and Shanghai Medicine and Health Development Foundation (No. 20221128), Shanghai Municipal Human Resources and Social Security Bureau (No. EK00000861).

Ethics approval statement

All animal experiments were approved by the Ethics Committee of Hainan Medical University.

CRediT authorship contribution statement

Chang Li: Investigation, Data curation. **Yi Cai:** Formal analysis, Data curation. **Yongmin Chen:** Data curation. **Jingyi Tong:** Data curation. **Youbin Li:** Data curation. **Dong Liu:** Data curation. **Yun Wang:** Data curation. **Zhiping Li:** Validation, Project administration. **Yan Wang:** Writing – original draft, Project administration. **Qifu Li:** Writing – review & editing, Project administration.

Declaration of competing interest

The authors declare that they have no known competing financial interests or personal relationships that could have appeared to influence the work reported in this paper.

Data availability

Data will be made available on request.

Abbreviation

ABC	ATP-binding cassette
ABCB1	ATP binding cassette subfamily B member 1
ABCG2	ATP binding cassette subfamily G member 2
ANOVA	One-way analysis of variance
APC	Allophycocyanin
ASM	Antiseizure medication
BBB	Blood-brain barrier
BPB	Blood-placental barrier
cDNA	Complementary DNA
COIP	Co-immunoprecipitation
CHOP	C/EBP-homologous protein
DAPI	4′, 6-diamidino-2-phenylindole
Ddrgk1	DDRGK domain containing protein 1
DEPs	Differentially expressed proteins
DIA-PASEF	Data-independent parallel accumulation serial fragmentation
FITC	Fluorescein isothiocyanate
GBP	Guanylate binding protein
GESA	Gene Set Enrichment Analysis
GO	Gene ontology
Grk5	G protein-coupled receptor kinase 5
H2DCFDA	2′,7′-dichlorofluorescin diacetate
HIF-1α	Hypoxia-inducible factor 1 subunit alpha
IBA1	Ionized calcium-binding adapter
Inmt	Indolethylamine *N*-methyltransferase
Irgm1	Immunity-related GTPase family M membrane 1
KA	Kainic acid
KEGG	Kyoto Encyclopedia of Genes and Genomes
LTG	Lamotrigine
LDH	Lactate dehydrogenase
LPS	Lipopolysaccharide
mTOR	Mammalian target of rapamycin
MTLE	Mesial temporal lobe epilepsy
NES	Normalized enrichment scores
NeuN	Neuronal nuclei
GFAP	Glial fibrillary acidic protein
PBS	Phosphate-buffered saline
PE	Phycoerythrin
PPE	Protein-protein interaction
PTZ	Pentylenetetrazole
qPCR	Quantitative real-time PCR
RAPA	Rapamycin
Rbm41	RNA binding motif protein 41
STAT1	Signal transducer and activator of transcription 1
Tgtp2	T-cell specific GTPase 2
TOF	Time-of-flight
WB	Western blot
WT	Wildtype

Appendix A. Supplementary data

Supplementary data to this article can be found online at https://doi.org/10.1016/j.redox.2024.103262.

References

[1] A. Pitkanen, X. Ekolle Ndode-Ekane, N. Lapinlampi, N. Puhakka, Epilepsy biomarkers - toward etiology and pathology specificity, Neurobiol. Dis. 123 (2019) 42–58. https://www.ncbi.nlm.nih.gov/pubmed/29782966.

[2] A. Hosomi, T. Nakanishi, T. Fujita, I. Tamai, Extra-renal elimination of uric acid via intestinal efflux transporter BCRP/ABCG2, PLoS One 7 (2012) e30456. https://www.ncbi.nlm.nih.gov/pubmed/22348008.

[3] W. Li, R.W. Sparidans, M.L.F. Martins, M. El-Lari, M.C. Lebre, O. van Tellingen, J. H. Beijnen, A.H. Schinkel, ABCB1 and ABCG2 restrict brain and testis accumulation and, alongside CYP3A, limit oral availability of the novel TRK inhibitor selitrectinib, Mol. Cancer Therapeut. 20 (2021) 1173–1182. https://www.ncbi.nlm.nih.gov/pubmed/33785654.

[4] R. Shawahna, Y. Uchida, X. Decleves, S. Ohtsuki, S. Yousif, S. Dauchy, A. Jacob, F. Chassoux, C. Daumas-Duport, P.O. Couraud, et al., Transcriptomic and quantitative proteomic analysis of transporters and drug metabolizing enzymes in freshly isolated human brain microvessels, Mol. Pharm. 8 (2011) 1332–1341. https://www.ncbi.nlm.nih.gov/pubmed/21707071.

[5] L.A. Doyle, W. Yang, L.V. Abruzzo, T. Krogmann, Y. Gao, A.K. Rishi, D.D. Ross, A multidrug resistance transporter from human MCF-7 breast cancer cells, Proc. Natl. Acad. Sci. U. S. A. 95 (1998) 15665–15670. https://www.ncbi.nlm.nih.gov/pubmed/9861027.

[6] S.F. Mousavi, K. Hasanpour, M. Nazarzadeh, A. Adli, M.S. Bazghandi, A. Asadi, A. Rad, O. Gholami, ABCG2, SCN1A and CYP3A5 genes polymorphism and drug-resistant epilepsy in children: a case-control study, Seizure 97 (2022) 58–62. https://www.ncbi.nlm.nih.gov/pubmed/35338956.

[7] S.A. Harby, N.A. Khalil, N.S. El-Sayed, E.H. Thabet, S.R. Saleh, M.H. Fathelbab, Implications of BCRP modulation on PTZ-induced seizures in mice: role of ko143 and metformin as adjuvants to lamotrigine, Naunyn-Schmiedeberg's Arch. Pharmacol. 396 (2023) 2627–2636. https://www.ncbi.nlm.nih.gov/pubmed/37067582.

[8] E. Aronica, J.A. Gorter, S. Redeker, E.A. van Vliet, M. Ramkema, G.L. Scheffer, R. J. Scheper, P. van der Valk, S. Leenstra, J.C. Baayen, et al., Localization of breast cancer resistance protein (BCRP) in microvessel endothelium of human control and epileptic brain, Epilepsia 46 (2005) 849–857. https://www.ncbi.nlm.nih.gov/pubmed/15946326.

[9] K. Romermann, R. Helmer, W. Loscher, The antiepileptic drug lamotrigine is a substrate of mouse and human breast cancer resistance protein (ABCG2), Neuropharmacology 93 (2015) 7–14. https://www.ncbi.nlm.nih.gov/pubmed/25645391.

[10] D.W. Kim, S.K. Lee, K. Chu, I.J. Jang, K.S. Yu, J.Y. Cho, S.J. Kim, Lack of association between ABCB1, ABCG2, and ABCC2 genetic polymorphisms and multidrug resistance in partial epilepsy, Epilepsy Res. 84 (2009) 86–90. https://www.ncbi.nlm.nih.gov/pubmed/19167193.

[11] P. Kwan, V. Wong, P.W. Ng, C.H. Lui, N.C. Sin, K.S. Wong, L. Baum, Gene-wide tagging study of the association between ABCC2, ABCC5 and ABCG2 genetic polymorphisms and multidrug resistance in epilepsy, Pharmacogenomics 12 (2011) 319–325. https://www.ncbi.nlm.nih.gov/pubmed/21449672.

[12] S.M. Sisodiya, L. Martinian, G.L. Scheffer, P. van der Valk, J.H. Cross, R.J. Scheper, B.N. Harding, M. Thom, Major vault protein, a marker of drug resistance, is upregulated in refractory epilepsy, Epilepsia 44 (2003) 1388–1396. https://www.ncbi.nlm.nih.gov/pubmed/14636345.

[13] L.D. Weidner, P. Kannan, N. Mitsios, S.J. Kang, M.D. Hall, W.H. Theodore, R. B. Innis, J. Mulder, The expression of inflammatory markers and their potential influence on efflux transporters in drug-resistant mesial temporal lobe epilepsy tissue, Epilepsia 59 (2018) 1507–1517. https://www.ncbi.nlm.nih.gov/pubmed/30030837.

[14] N. Percie du Sert, V. Hurst, A. Ahluwalia, S. Alam, M.T. Avey, M. Baker, W. J. Browne, A. Clark, I.C. Cuthill, U. Dirnagl, et al., The ARRIVE guidelines 2.0: updated guidelines for reporting animal research, Br. J. Pharmacol. 177 (2020) 3617–3624. https://www.ncbi.nlm.nih.gov/pubmed/32662519.

[15] R.J. Racine, Modification of seizure activity by electrical stimulation. II. Motor seizure, Electroencephalogr. Clin. Neurophysiol. 32 (1972) 281–294. https://www.ncbi.nlm.nih.gov/pubmed/4110397.

[16] M.N. Huizenga, E. Wicker, V.C. Beck, P.A. Forcelli, Anticonvulsant effect of cannabinoid receptor agonists in models of seizures in developing rats, Epilepsia 58 (2017) 1593–1602. https://www.ncbi.nlm.nih.gov/pubmed/28691158.

[17] A. Dhir, Pentylenetetrazol (PTZ) kindling model of epilepsy, Curr Protoc Neurosci. Chapter 9 (2012). Unit9 37, https://www.ncbi.nlm.nih.gov/pubmed/23042503.

[18] Y. Wang, G. Wang, J. Tao, X. Li, L. Hu, Q. Li, J. Lu, Y. Li, Z. Li, Autophagy associated with the efficacy of valproic acid in PTZ-induced epileptic rats, Brain Res. 1745 (2020) 146923. https://www.ncbi.nlm.nih.gov/pubmed/32504548.

[19] R. Troubat, S. Leman, K. Pinchaud, A. Surget, P. Barone, S. Roger, A.M. Le Guisquet, B. Brizard, C. Belzung, V. Camus, Brain immune cells characterization in UCMS exposed P2X7 knock-out mouse, Brain Behav. Immun. 94 (2021) 159–174. https://www.ncbi.nlm.nih.gov/pubmed/33609652.

[20] J. Wang, Y. Sun, X. Zhang, H. Cai, C. Zhang, H. Qu, L. Liu, M. Zhang, J. Fu, J. Zhang, et al., Oxidative stress activates NORAD expression by H3K27ac and promotes oxaliplatin resistance in gastric cancer by enhancing autophagy flux via targeting the miR-433-3p, Cell Death Dis. 12 (2021) 90. https://www.ncbi.nlm.nih.gov/pubmed/33462197.

[21] Y. Wang, Y. Li, G. Wang, J. Lu, Z. Li, Overexpression of Homer1b/c induces valproic acid resistance in epilepsy, CNS Neurosci. Ther. 29 (2023) 331–343. https://www.ncbi.nlm.nih.gov/pubmed/36353757.

[22] T. Singh, A. Mishra, R.K. Goel, PTZ kindling model for epileptogenesis, refractory epilepsy, and associated comorbidities: relevance and reliability, Metab. Brain Dis. 36 (2021) 1573–1590. https://www.ncbi.nlm.nih.gov/pubmed/34427842.
[23] K.C. Somera-Molina, B. Robin, C.A. Somera, C. Anderson, C. Stine, S. Koh, H. A. Behanna, L.J. Van Eldik, D.M. Watterson, M.S. Wainwright, Glial activation links early-life seizures and long-term neurologic dysfunction: evidence using a small molecule inhibitor of proinflammatory cytokine upregulation, Epilepsia 48 (2007) 1785–1800. https://www.ncbi.nlm.nih.gov/pubmed/17521344.
[24] P. Kumar, A. Lim, S.N. Hazirah, C.J.H. Chua, A. Ngoh, S.L. Poh, T.H. Yeo, J. Lim, S. Ling, N.B. Sutamam, et al., Single-cell transcriptomics and surface epitope detection in human brain epileptic lesions identifies pro-inflammatory signaling, Nat. Neurosci. 25 (2022) 956–966. https://www.ncbi.nlm.nih.gov/pubmed/35739273.
[25] S.H. Barghout, A. Aman, K. Nouri, Z. Blatman, K. Arevalo, G.E. Thomas, N. MacLean, R. Hurren, T. Ketela, M. Saini, et al., A genome-wide CRISPR/Cas9 screen in acute myeloid leukemia cells identifies regulators of TAK-243 sensitivity, JCI Insight 6 (2021). https://www.ncbi.nlm.nih.gov/pubmed/33476303.
[26] Y. Zuo, Q. Feng, L. Jin, F. Huang, Y. Miao, J. Liu, Y. Xu, X. Chen, H. Zhang, T. Guo, et al., Regulation of the linear ubiquitination of STAT1 controls antiviral interferon signaling, Nat. Commun. 11 (2020) 1146. https://www.ncbi.nlm.nih.gov/pubmed/32123171.
[27] F. Baran-Marszak, J. Feuillard, I. Najjar, C. Le Clorennec, J.M. Bechet, I. Dusanter-Fourt, G.W. Bornkamm, M. Raphael, R. Fagard, Differential roles of STAT1alpha and STAT1beta in fludarabine-induced cell cycle arrest and apoptosis in human B cells, Blood 104 (2004) 2475–2483. https://www.ncbi.nlm.nih.gov/pubmed/15217838.
[28] X. Hu, C. Herrero, W.P. Li, T.T. Antoniv, E. Falck-Pedersen, A.E. Koch, J.M. Woods, G.K. Haines, L.B. Ivashkiv, Sensitization of IFN-gamma Jak-STAT signaling during macrophage activation, Nat. Immunol. 3 (2002) 859–866. https://www.ncbi.nlm.nih.gov/pubmed/12172544.
[29] X.F. Zhao, Y. Liao, M.M. Alam, R. Mathur, P. Feustel, J.E. Mazurkiewicz, M. A. Adamo, X.C. Zhu, Y. Huang, Microglial mTOR is neuronal protective and antiepileptogenic in the pilocarpine model of temporal lobe epilepsy, J. Neurosci. 40 (2020) 7593–7608. https://www.ncbi.nlm.nih.gov/pubmed/32868461.
[30] X. Zhang, L. Li, Y. Li, Z. Li, W. Zhai, Q. Sun, X. Yang, M. Roth, S. Lu, mTOR regulates PRMT1 expression and mitochondrial mass through STAT1 phosphorylation in hepatic cell, Biochim. Biophys. Acta Mol. Cell Res. 1868 (2021) 119017. https://www.ncbi.nlm.nih.gov/pubmed/33741434.
[31] A. Jakobs, J. Koehnke, F. Himstedt, M. Funk, B. Korn, M. Gaestel, R. Niedenthal, Ubc9 fusion-directed SUMOylation (UFDS): a method to analyze function of protein SUMOylation, Nat. Methods 4 (2007) 245–250. https://www.ncbi.nlm.nih.gov/pubmed/17277783.
[32] L. Feng, W. Li, X. Li, X. Li, Y. Ran, X. Yang, Z. Deng, H. Li, N-MYC-interacting protein enhances type II interferon signaling by inhibiting STAT1 sumoylation, Faseb. J. 37 (2023) e23281. https://www.ncbi.nlm.nih.gov/pubmed/37933920.
[33] M.P. Malakhov, K.I. Kim, O.A. Malakhova, B.S. Jacobs, E.C. Borden, D.E. Zhang, High-throughput immunoblotting. Ubiquitiin-like protein ISG15 modifies key regulators of signal transduction, J. Biol. Chem. 278 (2003) 16608–16613. https://www.ncbi.nlm.nih.gov/pubmed/12582176.
[34] Y. Zhang, F. Thery, N.C. Wu, E.K. Luhmann, O. Dussurget, M. Foecke, C. Bredow, D. Jimenez-Fernandez, K. Leandro, A. Beling, et al., The in vivo ISGylome links ISG15 to metabolic pathways and autophagy upon Listeria monocytogenes infection, Nat. Commun. 10 (2019) 5383. https://www.ncbi.nlm.nih.gov/pubmed/31772204.
[35] A.A. Kazi, R.A. Gilani, A.J. Schech, S. Chumsri, G. Sabnis, P. Shah, O. Goloubeva, S. Kronsberg, A.H. Brodie, Nonhypoxic regulation and role of hypoxia-inducible factor 1 in aromatase inhibitor resistant breast cancer, Breast Cancer Res. 16 (2014) R15. https://www.ncbi.nlm.nih.gov/pubmed/24472707.
[36] H.C. Chen, H.K. Sytwu, J.L. Chang, H.W. Wang, H.K. Chen, B.H. Kang, D.W. Liu, C. H. Chen, T.T. Chao, C.H. Wang, Hypoxia enhances the stemness markers of cochlear stem/progenitor cells and expands sphere formation through activation of hypoxia-inducible factor-1 alpha, Hear. Res. 275 (2011) 43–52. https://www.ncbi.nlm.nih.gov/pubmed/21147209.
[37] A. Martinez-Chavez, N.H.C. Loos, M.C. Lebre, M.M. Tibben, H. Rosing, J. H. Beijnen, A.H. Schinkel, ABCB1 and ABCG2 limit brain penetration and, together with CYP3A4, total plasma exposure of abemaciclib and its active metabolites, Pharmacol. Res. 178 (2022) 105954. https://www.ncbi.nlm.nih.gov/pubmed/34700018.
[38] Y.K. Song, M.J. Kim, M.S. Kim, J.H. Lee, S.J. Chung, J.S. Song, Y.J. Chae, K.R. Lee, Role of the efflux transporters Abcb1 and Abcg2 in the brain distribution of olaparib in mice, Eur. J. Pharmaceut. Sci. 173 (2022) 106177. https://www.ncbi.nlm.nih.gov/pubmed/35341895.
[39] Dixit A. Banerjee, D. Sharma, A. Srivastava, J. Banerjee, M. Tripathi, D. Prakash, P. Sarat Chandra, Upregulation of breast cancer resistance protein and major vault protein in drug resistant epilepsy, Seizure 47 (2017) 9–12. https://www.ncbi.nlm.nih.gov/pubmed/28273590.
[40] I.F. Emery, A. Gopalan, S. Wood, K.H. Chow, C. Battelli, J. George, H. Blaszyk, J. Florman, K. Yun, Expression and function of ABCG2 and XIAP in glioblastomas, J. Neuro Oncol. 133 (2017) 47–57. https://www.ncbi.nlm.nih.gov/pubmed/28432589.
[41] M.R. Jablonski, D.A. Jacob, C. Campos, D.S. Miller, N.J. Maragakis, P. Pasinelli, D. Trotti, Selective increase of two ABC drug efflux transporters at the blood-spinal cord barrier suggests induced pharmacoresistance in ALS, Neurobiol. Dis. 47 (2012) 194–200. https://www.ncbi.nlm.nih.gov/pubmed/22521463.
[42] J.Y. Liu, M. Thom, C.B. Catarino, L. Martinian, D. Figarella-Branger, F. Bartolomei, M. Koepp, S.M. Sisodiya, Neuropathology of the blood-brain barrier and pharmaco-resistance in human epilepsy, Brain 135 (2012) 3115–3133. https://www.ncbi.nlm.nih.gov/pubmed/22750659.
[43] S. Puttachary, S. Sharma, A. Thippeswamy, T. Thippeswamy, Immediate epileptogenesis: impact on brain in C57BL/6J mouse kainate model, Front Biosci (Elite Ed) 8 (2016) 390–411. https://www.ncbi.nlm.nih.gov/pubmed/27100347.
[44] C.J. Gibson, M.M. Hossain, J.R. Richardson, L.M. Aleksunes, Inflammatory regulation of ATP binding cassette efflux transporter expression and function in microglia, J. Pharmacol. Exp. Therapeut. 343 (2012) 650–660. https://www.ncbi.nlm.nih.gov/pubmed/22942241.
[45] B. Poller, J. Drewe, S. Krahenbuhl, J. Huwyler, H. Gutmann, Regulation of BCRP (ABCG2) and P-glycoprotein (ABCB1) by cytokines in a model of the human blood-brain barrier, Cell. Mol. Neurobiol. 30 (2010) 63–70. https://www.ncbi.nlm.nih.gov/pubmed/19629677.
[46] S. Yousif, C. Chaves, S. Potin, I. Margaill, J.M. Scherrmann, X. Decleves, Induction of P-glycoprotein and Bcrp at the rat blood-brain barrier following a subchronic morphine treatment is mediated through NMDA/COX-2 activation, J. Neurochem. 123 (2012) 491–503. https://www.ncbi.nlm.nih.gov/pubmed/22845665.
[47] J.D. Salvamoser, J. Avemary, H. Luna-Munguia, B. Pascher, T. Getzinger, T. Pieper, M. Kudernatsch, G. Kluger, H. Potschka, Glutamate-mediated down-regulation of the multidrug-resistance protein BCRP/ABCG2 in porcine and human brain capillaries, Mol. Pharm. 12 (2015) 2049–2060. https://www.ncbi.nlm.nih.gov/pubmed/25898179.
[48] H.F. Bradford, Glutamate, GABA and epilepsy, Prog. Neurobiol. 47 (1995) 477–511. https://www.ncbi.nlm.nih.gov/pubmed/8787032.
[49] M.T. Yang, Y.C. Lin, W.H. Ho, C.L. Liu, W.T. Lee, Everolimus is better than rapamycin in attenuating neuroinflammation in kainic acid-induced seizures, J. Neuroinflammation 14 (2017) 15. https://www.ncbi.nlm.nih.gov/pubmed/28109197.
[50] S. Shen, D. Callaghan, C. Juzwik, H. Xiong, P. Huang, W. Zhang, ABCG2 reduces ROS-mediated toxicity and inflammation: a potential role in Alzheimer's disease, J. Neurochem. 114 (2010) 1590–1604. https://www.ncbi.nlm.nih.gov/pubmed/20626554.
[51] F. Mosaffa, H. Lage, J.T. Afshari, J. Behravan, Interleukin-1 beta and tumor necrosis factor-alpha increase ABCG2 expression in MCF-7 breast carcinoma cell line and its mitoxantrone-resistant derivative, MCF-7/MX, Inflamm. Res. 58 (2009) 669–676. https://www.ncbi.nlm.nih.gov/pubmed/19333723.
[52] Y. Zeng, D. Callaghan, H. Xiong, Z. Yang, P. Huang, W. Zhang, Abcg2 deficiency augments oxidative stress and cognitive deficits in Tg-SwDI transgenic mice, J. Neurochem. 122 (2012) 456–469. https://www.ncbi.nlm.nih.gov/pubmed/22578166.
[53] N. Nakamichi, E. Morii, J. Ikeda, Y. Qiu, S. Mamato, T. Tian, S. Fukuhara, K. Aozasa, Synergistic effect of interleukin-6 and endoplasmic reticulum stress inducers on the high level of ABCG2 expression in plasma cells, Lab. Invest. 89 (2009) 327–336. https://www.ncbi.nlm.nih.gov/pubmed/19139722.
[54] J.S. Choi, S.Y. Kim, H.J. Park, J.H. Cha, Y.S. Choi, J.E. Kang, J.W. Chung, M. H. Chun, M.Y. Lee, Upregulation of gp130 and differential activation of STAT and p42/44 MAPK in the rat hippocampus following kainic acid-induced seizures, Brain. Res. Mol. Brain Res. 119 (2003) 10–18. https://www.ncbi.nlm.nih.gov/pubmed/14597225.
[55] E. Dashtban-Moghadam, S. Khodaverdian, B. Dabirmanesh, J. Mirnajafi-Zadeh, A. Shojaei, M. Mirzaie, P. Choopanian, M. Atabakhshi-Kashi, Y. Fatholahi, K. Khajeh, Hippocampal tandem mass tag (TMT) proteomics analysis during kindling epileptogenesis in rat, Brain Res. 1822 (2024) 148620. https://www.ncbi.nlm.nih.gov/pubmed/37848119.
[56] M. Chatterjee-Kishore, K.L. Wright, J.P. Ting, G.R. Stark, How Stat1 mediates constitutive gene expression: a complex of unphosphorylated Stat1 and IRF1 supports transcription of the LMP2 gene, EMBO J. 19 (2000) 4111–4122. https://www.ncbi.nlm.nih.gov/pubmed/10921891.
[57] H. Cheon, G.R. Stark, Unphosphorylated STAT1 prolongs the expression of interferon-induced immune regulatory genes, Proc. Natl. Acad. Sci. U. S. A. 106 (2009) 9373–9378. https://www.ncbi.nlm.nih.gov/pubmed/19478064.
[58] X. Xue, X. Tian, C. Zhang, Y. Miao, Y. Wang, Y. Peng, S. Qiu, H. Wang, J. Cui, L. Cao, et al., YAP ISGylation increases its stability and promotes its positive regulation on PPP by stimulating 6PGL transcription, Cell Death Dis. 8 (2022) 59. https://www.ncbi.nlm.nih.gov/pubmed/35149670.
[59] X. Zhang, D. Bogunovic, B. Payelle-Brogard, V. Francois-Newton, S.D. Speer, C. Yuan, S. Volpi, Z. Li, O. Sanal, D. Mansouri, et al., Human intracellular ISG15 prevents interferon-alpha/beta over-amplification and auto-inflammation, Nature 517 (2015) 89–93. https://www.ncbi.nlm.nih.gov/pubmed/25307056.
[60] P. Przanowski, S. Loska, D. Cysewski, M. Dabrowski, B. Kaminska, ISG'ylation increases stability of numerous proteins including Stat1, which prevents premature termination of immune response in LPS-stimulated microglia, Neurochem. Int. 112 (2018) 227–233. https://www.ncbi.nlm.nih.gov/pubmed/28774718.
[61] M. Urbanska, A. Gozdz, M. Macias, I.A. Cymerman, E. Liszewska, I. Kondratiuk, H. Devijver, B. Lechat, F. Van Leuven, J. Jaworski, GSK3beta controls mTOR and prosurvival signaling in neurons, Mol. Neurobiol. 55 (2018) 6050–6062. https://www.ncbi.nlm.nih.gov/pubmed/29143288.
[62] Y. Xu, C. Liu, S. Chen, Y. Ye, M. Guo, Q. Ren, L. Liu, H. Zhang, C. Xu, Q. Zhou, et al., Activation of AMPK and inactivation of Akt result in suppression of mTOR-mediated S6K1 and 4E-BP1 pathways leading to neuronal cell death in in vitro models of Parkinson's disease, Cell. Signal. 26 (2014) 1680–1689. https://www.ncbi.nlm.nih.gov/pubmed/24726895.
[63] E.D. Smith, G.A. Prieto, L. Tong, I. Sears-Kraxberger, J.D. Rice, O. Steward, C. W. Cotman, Rapamycin and interleukin-1beta impair brain-derived neurotrophic factor-dependent neuron survival by modulating autophagy, J. Biol. Chem. 289 (2014) 20615–20629. https://www.ncbi.nlm.nih.gov/pubmed/24917666.